AD 738493

D D C
RECEIVED
MAR 17 1972
C

Reproduced by
NATIONAL TECHNICAL
INFORMATION SERVICE
Springfield, Va. 22151

Unclassified

Security Classification

DOCUMENT CONTROL DATA - R & D

(Security classification of title, body of abstract and indexing annotation must be entered when the overall report is classified)

1. ORIGINATING ACTIVITY (Corporate author)

Lockheed Missiles & Space Company
Sunnyvale, California 94088

2a. REPORT SECURITY CLASSIFICATION

Unclassified

2b. GROUP

3. REPORT TITLE

EXPERIMENTAL INVESTIGATION OF THE VENTILATION OF VERTICAL SURFACE-PIERCING STRUTS IN THE PRESENCE OF CAVITATION

4. DESCRIPTIVE NOTES (Type of report and inclusive dates)

Final Report November 1966-March 1968

5. AUTHOR(S) (First name, middle initial, last name)

Robert L. Waid

6. REPORT DATE

May 1968

7a. TOTAL NO. OF PAGES

65

7b. NO. OF REFS

16

8a. CONTRACT OR GRANT NO

N00014-67-C-0222

b. PROJECT NO.

c.

d.

9a. ORIGINATOR'S REPORT NUMBER(S)

LMSC/D019597

9b. OTHER REPORT NO(S) (Any other numbers that may be assigned this report)

10. DISTRIBUTION STATEMENT

Approved for Public Release: Distribution Unlimited

11. SUPPLEMENTARY NOTES

12. SPONSORING MILITARY ACTIVITY

Naval Ship Research and Development Center
Office of Naval Research

13. ABSTRACT

An experimental program was conducted in the Lockheed Underwater Missile Facility to determine the mechanism, characteristics, and the significant parameters controlling ventilation in the presence of cavitation for three streamlined, vertically, surface-piercing strut models. Tests were performed for speeds from 20 to 30 fps, for yaw angles from 6 to 10 degrees, for submergences of 1 to 1.5 chord lengths. The radius of the leading edge of the struts ranged from 0 to 0.0327 chord lengths. Forces were measured and flow photographs were obtained. The importance of vapor cavitation number as the principal parameter influencing the inception of ventilation was demonstrated. Mechanisms for inception were observed and are described. The larger the nose radius the higher was the vapor cavitation number for ventilation inception and the greater was the reversal of the side force when ventilation was complete.

DD FORM 1 NOV 65 1473

Unclassified

Security Classification

Unclassified
Security Classification

14. KEY WORDS	LINK A ROLE	LINK A WT	LINK B ROLE	LINK B WT	LINK C ROLE	LINK C WT
Strut						
Ventilation						
Cavitation						
Strut ventilation						

Unclassified
Security Classification

Final Report

EXPERIMENTAL INVESTIGATION OF THE VENTILATION OF VERTICAL SURFACE-PIERCING STRUTS IN THE PRESENCE OF CAVITATION

May 1968 LMSC/D019597

Prepared by

Robert L. Waid

This research was carried out under the
Naval Ship Systems Command
Hydrofoil Advanced Development Program S46-06,
Administered by the Naval Ship Research and Development Center
Office of Naval Research Contract N00014-67-C-0222

Approved for Public Release: Distribution Unlimited

LOCKHEED MISSILES & SPACE COMPANY

TABLE OF CONTENTS

Section	Title	Page
	SUMMARY	i
	LIST OF FIGURES	ii
	NOMENCLATURE	v
1.	INTRODUCTION	1
2.	MODEL DESCRIPTION	3
3.	TEST EQUIPMENT DESCRIPTION	4
4.	TEST PROCEDURES	5
5.	DATA REDUCTION PROCEDURES	7
6.	ACCURACY AND REPEATABILITY	8
7.	RESULTS AND DISCUSSION	9
7.1	Ventilation Characteristics	9
7.2	Conditions for Inception of Ventilation	14
7.3	Measured Forces	16
8.	CONCLUSIONS AND RECOMMENDATIONS	19
9.	REFERENCES	22
	TABLE I	24
	Coordinates of Leading Edge of Strut Models	
	FIGURES 1-31	

SUMMARY

An experimental program was conducted in the Lockheed Underwater Missile Facility to determine the mechanism, characteristics, and the significant parameters controlling ventilation in the presence of cavitation for three streamlined, vertically, surface-piercing strut models. Tests were performed for speeds from 20 to 30 fps, for yaw angles from 6 to 10 degrees, for submergences of 1 to 1.5 chord lengths. The radius of the leading edge of the struts ranged from 0 to 0.0327 chord lengths. Forces were measured and flow photographs were obtained. The importance of vapor cavitation number as the principal parameter influencing the inception of ventilation was demonstrated. Mechanisms for inception were observed and are described. The larger the nose radius the higher was the vapor cavitation number for ventilation inception and the greater was the reversal of the side force when ventilation was complete.

LIST OF FIGURES

Number	Title	Page
1.	Physical characteristics of strut models	25
2.	Photograph of towing carriage with strut model installed	26
3.	Photograph of strut model installation on force balance and elevating mechanism	27
4.	Cavitation on strut model 0 at a yaw angle of -8 degrees	28
5.	Inception of ventilation on strut model 0 at a yaw angle of -8 degrees	29
6.	Fully developed ventilation on strut model 0 at a yaw angle of -8 degrees	30
7.	Strip of motion picture film showing ventilation inception and transition for strut model 2 at a yaw angle of -8 degrees and a speed of 30 fps. (Time between successive frames was 0.01 seconds)	31
8.	Elevation of the surface of the water adjacent to strut model at a yaw angle of -10 degrees for noncavitating conditions.	34
9.	Underwater photograph of strut model 0 at a yaw angle of -8 degrees	35
10.	Underwater photograph of strut model 3 at a yaw angle of -6 degrees	36
11.	Water surface and upper cavity boundary for strut model 0 at -8 degrees yaw angle for a speed of 30 fps. (Water surface elevation with no cavitation is shown for reference)	37
12.	Water surface and upper cavity boundary for strut model 0 at -8 degrees yaw angle for a speed of 30 fps and a surface vapor cavitation number of 0.24	38
13.	Sketch of mechanism for inception of surface ventilation of a yawed strut through filament-like vortex cores	39
14.	Force and cavitation characteristics during ventilation transition of strut model 2 at a yaw angle of -8 degrees for a speed of 30 fps and a surface vapor cavitation number of 0.293	40

LIST OF FIGURES (continued)

Number	Title	Page
15.	Conditions of flow for strut model 0 at a yaw angle of -8 degrees and a submergence of 1.0 chords (Solid symbol indicates ventilation)	41
16.	Conditions of flow for strut model 2 at a yaw angle of -6 degrees and a submergence of 1.0 chords. (Solid symbol indicates ventilation)	42
17.	Conditions of flow for strut model 2 at a yaw angle of -8 degrees and a submergence of 1.0 chords. (Solid symbol indicates ventilation)	43
18.	Conditions of flow for strut model 2 at a yaw angle of -10 degrees and a submergence of 1.0 chords. (Solid symbol indicates ventilation)	44
19.	Conditions of flow for strut model 2 at a yaw angle of -8 degrees and a submergence of 1.5 chords. (Solid symbol indicates ventilation)	45
20.	Conditions of flow for strut model 3 at a yaw angle of -6 degrees and a submergence of 1.0 chords. (Solid symbol indicates ventilation)	46
21.	Conditions of flow for strut model 3 at a yaw angle of -8 degrees and a submergence of 1.0 chords. (Solid symbol indicates ventilation)	47
22.	Conditions for ventilation inception of strut model 2 based on the vapor cavitation number at a representative depth (0.1 chord lengths). (Solid symbols indicates ventilation)	48
23.	Vapor cavitation number for incipient ventilation at a submergence of 1.0 chord lengths.	49
24.	Side force and drag coefficient for strut model 0 at a yaw angle of -8 degrees and a submergence of 1.0 chord lengths	50
25.	Side force and drag coefficient for strut model 2 at a yaw angle of -6 degrees and a submergence of 1.0 chord lengths	51
26.	Side force and drag coefficient for strut model 2 at a yaw angle of -8 degrees and a submergence of 1.0 chord lengths	52
27.	Side force and drag coefficient for strut model 2 at a yaw angle of -10 degrees and a submergence of 1.0 chord lengths	53

LIST OF FIGURES (concluded)

Number	Title	Page
28.	Side force and drag coefficient for strut model 2 at a yaw angle of -8 degrees and a submergence of 1.5 chord lengths	54
29.	Side force and drag coefficient for strut model 3 at a yaw angle of -6 degrees and a submergence of 1.0 chord lengths	55
30.	Side force and drag coefficient for strut model 3 at a yaw angle of -8 degrees and a submergence of 1.0 chord lengths	56
31.	Average side force coefficients as a function of yaw angle for strut models, 0, 2, and 3 at a submergence of 1.0 chord lengths for a velocity of 30 feet per second. ($F_N = 5.3$)	57

NOMENCLATURE

A	ch	Submerged planform area of strut model
c	1.00	Chord of strut model hydrofoil (ft)
C_D	$\frac{D}{\frac{1}{2}\rho V^2 A}$	Drag coefficient
C_S	$\frac{S}{\frac{1}{2}\rho V^2 A}$	Side force coefficient
D		Drag force (lbs)
F	$\frac{V}{\sqrt{gc}}$	Froude number
g	32.150	Acceleration of gravity at LJMF (ft/sec^2)
h		Depth of submergence of bottom edge of strut model (ft)
h_R		Representative depth for cavitation number (ft)
S		Side force (lbs)
P_a		Pressure of air above surface of water (psia)
P_v		Vapor pressure of water (psia)
Re	$\frac{cV}{\nu}$	Reynolds number
V		Speed of carriage (ft/sec)
ρ		Density of water (slugs/ft^3)

NOMENCLATURE (Continued)

σ_{vs}	$\dfrac{(P_a - P_v)\,144}{\frac{1}{2}\rho V^2}$	Vapor cavitation number at the surface of the water
σ_{vr}	$\dfrac{\rho g h_R + 144(P_a - P_v)}{\frac{1}{2}\rho V^2}$	Representative vapor cavitation number
ν		Kinematic viscosity of water (ft^2/sec)

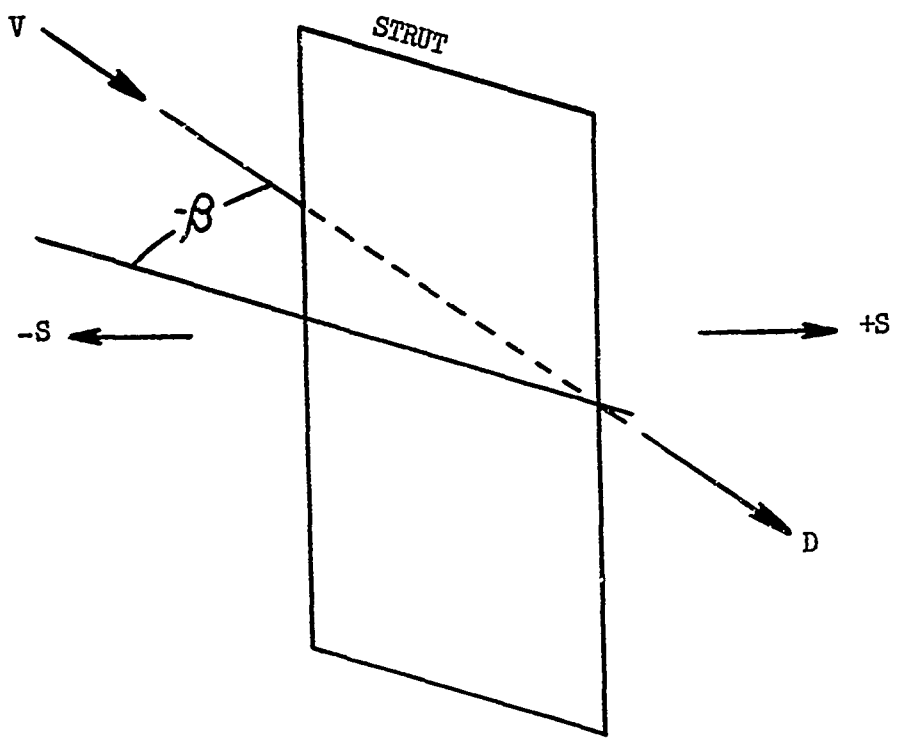

1. INTRODUCTION

The phenomenon of ventilation of above-surface air through the surface and into water has been studied for a wide variety of configurations by numerous investigators. Summaries of these efforts are found in References 1-3*. The preponderance of experimental work in this area is the result of the complex interactions of free surface, boundary layer, cavitation, and surface-tension effects on ventilation. These interactions preclude development of appropriate mathematical models. Although the variety of test conditions and configurations used in these studies has been large, they are, unfortunately, in restrictive combinations which are dictated by the capabilities of each respective test facility. The widespread application of the conclusions based on these small-scale results is necessarily provisional. It is important to note that for full-scale conditions in which ventilation is of potential significance, the presence of cavitation can also be expected. Since most of the existing data do not include cavitation, the application of ventilation criteria must make adequate consideration for the effects of cavitation--the subject of this study.

The study of ventilation phenomena is generally considered in two areas, (1) the avoidance of ventilation and (2) the occurrence and use of ventilation. In this study the avoidance of ventilation is the principal area of concern.

In this area, development effort is usually concentrated on determining the critical shape, arrangement, boundary layer condition, placement of devices (fences), and safe limits of speed and angle-of-attack operation. The purpose is to avoid any ventilation, regardless of how it is initiated. Some analyses[1,2] have shown a reasonable ventilation inception mechanism based on laminar-boundary-layer separation. Unfortunately, the hypothesized mechanism is incomplete, since there is no method proposed which describes the initiation of ventilation from the free surface to the separated region in the boundary layer which occurs somewhere below the free surface. In fact, rough water test conditions have been utilized[5] to provide an artificial method of initiating ventilation into the separated boundary layer for yaw angles of less than

*References are found on page 22.

24 degrees for 2- and 3-inch chord models. Without this technique, large hysterisis of inception occurred, as has been noted by many observers.[1-3] There has been considerable success in correlating various break points in the ventilation speed for various yaw angles, when compared over a Froude number range of 2 to 6. Because of the use of atmospheric test facilities, tests in the 2 to 6 Froude number range have no cavitation, and in fact require large angles to effect ventilation inception. These large angles produce large pressure gradients which encourage separation of the thin laminar boundary layer occurring at these low velocities on small models. If cavitation can be made to occur at lower angles of attack than those required for separation, then a cavitation mechanism of potential ventilation inception may occur.

It is noted that recent tests[6,7] of blunt-based, parabolic struts at small yaw angles, have shown leading edge cavities which became ventilated at high speeds and low cavitation numbers. In these cases the leading edge cavities became large and long, approaching both the free surface and the base cavity. It is not known whether the ventilation in these tests was initiated into the end of the cavity or through the spray sheet. Regardless of the mechanism, it is apparent that additional definitive information on the interaction of the free surface and cavitation on ventilation inception is required if ventilation is to be avoided.

The objective of this study was to determine the mechanism, characteristics, and the significant parameters controlling ventilation in the presence of cavitation for streamlined, surface-piercing struts in calm water. The parameters primarily examined were the cavitation number (for defining the extent and location of the cavitation), the submergence and angle of attack (for defining the effects of strut geometry), and the test speed (for defining the general flow field including the cavitation), the radius of the nose (for defining the effects of strut geometry), and the test speed (for defining the inertial characteristics of the free surface and the fluid layer between the surface and the cavitation). The same strut models tested at the Naval Ship Research and Development Center were utilized in this study to increase the

useful range of tested conditions and to eliminate ambiguous results which often occur between data obtained from different sets of models.

The following sections of this report present a description of the test program, the test data, and a discussion of the test results including a description of the most probable mechanism for ventilation of cavitation on yawed, surface-piercing struts.

2. MODEL DESCRIPTION

The three strut models which were tested had been fabricated for and previously tested at the Naval Ship Research and Development Center[8]. The struts were of rectangular planform with a 1-foot chord and a contoured length of approximately 4 feet. The physical characteristics of the struts, as designed, are presented in figure 1. The lower end of the struts were cut-off sharply normal to the span of the struts. The 12% maximum thickness of the struts occurred at the mid chord. The three struts were from a family of four struts designed to evaluate the effects of the radius at the leading edge of the strut, which ranged from 0 (circular arc section) to 0.0327 feet (3.27% chord). The three models selected to be tested in LUMF were done so on the basis of the widest expected range of useful results and with consideration of the somewhat oversized nose radius which had been machined on strut model 1. A circular arc was used for the section of the strut between the mid chord and the trailing edge. The included angle at the trailing edge of all the struts was 27.2 degrees, as was the included angle at the leading edge for the circular arc strut. The coordinates for the front half-chord length of the struts with finite leading edge radii were developed so that the profile had a continuous radius of curvature, convex outward, from the leading edge to the mid-chord. Table I presents the coordinates of the leading edge of the strut models. The models are designated 0, 1, 2, 3 in increasing order of radius at the leading edge. It is reported[8] that the struts, machined from stainless steel, differed from the specified offsets by less than $\pm$ 0.040 inch with surface waviness of less than $\pm$ 0.005 inch.

3. TEST EQUIPMENT DESCRIPTION

The test program was performed in the Lockheed Underwater Missile Facility utilizing the unique, controllable pressure above the surface of water of the towing tank. Details of the facility are available in Reference 4. Figure 2 shows the LUMF towing carriage with the strut model installed for testing.

The strut models were attached to the six-component, external force balance[9] by an adapter which allowed manual adjustment of the yaw angle of the strut. These tests were conducted with the strut models installed perpendicular to the water surface; i.e., without sweep or dihederal. The force balance was attached to the elevating mechanism which allowed remote adjustment of the depth of submergence of the struts. The installation on the force balance of the strut with the circular arc section is shown in Figure 3. The yaw angles during these tests were all negative, or leading edge to the port side. To minimize ambiquity with the struts and the yaw angle, the negative convention for the yaw angle has been maintained throughout this report.

The outputs from the force balance were routed to a recording oscillograph which produced oscillograms of the test data. The speed of the towing carriage, the location of the carriage, and a digitally-coded, time signal were also recorded on the oscillograms.

Four cameras were utilized to provide optical data for evaluation of the cavitation on the strut and the ventilation mechanism. A 70-mm camera, installed on the towing carriage, was aimed for a nearly plan view of the strut from an angle of approximately 40 degrees above the horizontal. This camera was automatically operated at 1 frame per second. A 16-mm camera was installed on the carriage adjacent to the 70-mm camera to operate at 100 frames per second to provide details of the entire flow field during the transition from cavitating to ventilating flow. A second 16-mm camera was mounted forward and lower than the other carriage cameras to obtain a better view of the critical region between the cavity wall and the water surface. This camera was operated at 200 frames per second to allow more resolution of the details

of ventilation inception. The fourth camera was installed in a viewing port located 2¼ feet below the water surface near the end of the run of the towing carriage. This 16-mm camera was operated at 200 frames per second to effectively stop the motion of the strut model as it passed the field of view. The 3 high-speed cameras were equipped with the same digitally-coded, time signal which was recorded on the oscillogram, so that all test data could be time-related to the details occurring during ventilation inception. The photographic data obtained were instrumental in confirming the details of the inception of ventilation and transition to full ventilation.

The possibility that the inception of ventilation might be difficult to experience in the short run time in LUMF led to development of a system to artificially aid and to forcefully cause ventilation. This system consisted of a submerged manifold of air jets which was located near the end of the stroke of the carriage launching catapult. The field of air bubbles which were blown into the water adjacent to the low pressure side of the strut effectively caused ventilation of the strut under most of the required conditions.

4. TEST PROCEDURES

Tests runs with the three strut models were performed in LUMF over a range of test speeds (20, 25 and 30 fps) with the pressure in the air above the surface of the water as the primary test parameter. The air pressure was varied from atmospheric to 1.3 psia providing a range in vapor cavitation numbers down to 0.162. The yaw angle of the strut models was set at -6, -8, and -10 degrees (leading edge to the port side). The submergence of the models was set at 1.0 and 1.5 chord lengths.

Two techniques were employed to determine the necessary conditions for the inception of ventilation. In both cases the strut model was at fixed yaw angles. The steady state technique was first used. In this case, the towing carriage was catapulted to a pre-set speed, and the carriage maintained that speed throughout the test run. If the conditions for strut ventilation were

imminent, ventilation could be expected to occur during the constant speed run. A coarse grid of test conditions (velocity and ambient pressure) was first surveyed to bracket the probable region for ventilation. A detailed study at intermediate conditions near inception was then planned.

In practice this technique was found to be very inadequate for the selection of critical test conditions that should be tested to determine inception. At -10 degrees yaw angle, strut model 2 ventilated while the strut was being accelerated by the catapults at 40 ft/sec^2 for cavitation numbers as high as 2.3. On the other extreme, the same strut was not ventilated at a cavitation number of 0.2 for a yaw angle of -6 degrees. The inability to obtain ventilation, as desired under these steady state conditions, led to the development of the second technique.

The unsteady, testing technique made use of the variable speed capability of the towing carriage to provide a slowly changing velocity and cavitation environment throughout the first half of the test run. The launching acceleration was terminated at approximately 5 fps below the desired steady speed and the carriage continued to accelerate at 2.6 ft/sec^2 to the pre-set speed. This avoided the occurrence of high accelerations in the vicinity of the critical ventilation conditions, which appeared to have been the primary cause of the premature ventilation. The slowly increasing speed of the carriage allowed a useful range of test conditions to be sampled during one test run, greatly enhancing the surveying rate. During the latter half of the test run, the constant speed allowed ventilation to occur under steady-state conditions which had been approached without large unsteady effects. The statistical nature of ventilation could then be studied. When ventilation was encountered by this method several tests were run at various final speeds to bracket the conditions for inception under both slowly accelerating and steady state conditions.

Standard testing procedures, as described in detail in Ref. 9, were employed for all other testing operations.

5. DATA REDUCTION PROCEDURES

All the data obtained by the external force balance and the several cameras were reviewed and analyzed with regard to applicability of the data to the determination of the mechanism and significant parameters controlling ventilation in the presence of cavitation.

The external force balance data were converted to engineering units and summarized to obtain the total side force and the drag force on the strut model. The forces on the strut were determined immediately prior to the onset of ventilation during the variable speed portion of the test and also during the steady-state test conditions. These forces were then reduced to standard, non-dimensional coefficients, based on the planform area of the portion of the strut which was submerged below the undisturbed water surface. These coefficients are defined in the section on nomenclature with the sign convention as noted there also. In this convention the non-ventilating strut model at a negative yaw angle develops a side force in the port direction which is also a negative sense. Upon ventilation, the side force reversed to the starboard direction for a positive sense.

The test speed was obtained by the determination of the time required for the towing carriage to travel a known distance, usually the entire constant speed portion of the test run. In that portion of the test with increasing speed, a short travel distance centered at the time of the force measurements was used to determine the average velocity.

The cavitation number that is considered to be most informative for the inception of ventilation from the surface into the cavity is based on the difference in pressure between the air above the surface and the pressure within the cavity. Since no pressure measurement capability was provided in these models, it has been assumed for the purposes of test description that the cavity pressure was the vapor pressure of the water at the temperature of the test. This parameter has been labelled the vapor cavitation number at the surface of the water, σ_{vs}.

Special measurements of various flow conditions observed in the optical data were obtained for numerous representative test conditions in support of the evaluation of the ventilation inception and transition mechanisms. These data are all presented in the discussion of the results of this study.

6. ACCURACY AND REPEATABILITY

The test data are estimated to have accuracies within the limits as shown below. The ranges of the measurements for this program are also shown in this table.

Measurement (units)	Range tested	Estimated Limits of Accuracy
Side force (lbs)	29 - 199	± 4
Drag force (lbs)	11 - 93	± 2
Tank air pressure (psia)	1.3 - 14.7	± .02
Tank water temperature (^{o}F)	57.2 - 57.4	± .2
Carriage velocity (fps)	20 - 31.4	± .02
Model depth of submergence (ft)	1 - 1.5	± .008
Model yaw angle (^{o})	6 - 10	± .05

The repeatability of the test conditions for this program was good, as shown by the ability to repeat the desired air pressure within ± 0.01 psid and to repeat average test speeds within ± 0.3 fps. Unsteady forces on the strut models caused by shedding of portions of the vapor cavities yielded large scatter in the measured force data.

7. RESULTS AND DISCUSSION

The test results have been analyzed from several different points of view so that these limited data can be most usefully applied in comparison with the other limited existing data in this area, and so that the nature of surface ventilation in the presence of cavitation can be understood. The first section presents a discussion of the flow conditions which were observed at the inception of ventilation and during the process of transition to full ventilation. The probable mechanism of ventilation is discussed relative to the observed data. The next section presents the conditions which were required for ventilation to occur and relates these to data from other sources. The final section of this discussion presents the summarized force data obtained during this program.

7.1 Ventilation Characteristics

The very limited data previously available shed little light on the surface ventilation of vertical struts in the presence of cavitation. The data obtained during the conduct of this experimental program have been sufficient to allow development of a detailed description of the mechanism of ventilation inception with cavitation.

Figures 4 through 6 present a typical series of photographs of the development of surface ventilation for strut model 0 (circular arc) at a yaw angle of -8 degrees. Figure 4 was obtained early in the test run when the flow field was dominated by the vapor-filled cavity originating at the leading edge of the strut. The other significant feature of the flow field is the spray sheet which climbs up the side of the strut. The height and shape of the spray sheet are functions of the model, chiefly the nose radius in our case, the yaw angle and the test speed. There is a distinctive row of highlights in photographs 4 and 5 which marks the approximate intersection of the thin spray sheet and the local surface of the water adjacent to the strut. This line roughly parallels the upper edge of the vapor-filled cavity. It should be of interest to note that near the quarter chord line the cavities extend above the undisturbed water surface as much as 0.15 chord lengths for

model 3. This cavity exists within the water pushed up by the strut, some of which later enters the spray sheet. The vapor cavity filling the tip vortex is readily seen. Because of its short length, the tip vortex is unable to penetrate the free surface leading to the conclusion that it is not a primary ventilation factor for these test conditions.

As the test speed is increased, the cavitation number decreases and the cavity grows in length and in height. Suddenly, there occurs a noticeable disturbance to the upper edge of the cavity and to the spray sheet intersection near the leading edge of the strut. Figure 7 presents a time history of the ventilation by 15 frames reproduced from the test film. The radical separation of the spray sheet between frames 4 and 8 is the basic clue as to the flow passage through which the ventilating air is entering the cavity. The cavity then rapidly grows out of the field of view and the forces on the strut become reversed. This is the ventilation phenomenon which will now be examined in detail.

The inception mechanism is intimately tied to the proximity of two surfaces; the local free water surface and the local cavity surface. The surface of the water immediately adjacent to the strut is displaced upwards to become the attached spray sheet. A small distance further away from the surface of the strut the water surface has been observed to be pushed up near the leading edge of the strut and to be drawn down near the trailing edge of the strut. These effects are illustrated in figure 8 for noncavitating conditions at speeds from 10 to 30 fps for a yaw angle of -8 degrees. These data were obtained from the underwater camera, and are plotted to show that the shape of the local water surface in the vicinity of the strut is reasonably independent of the test speed in the absence of cavitation. The shape of the water surface in the wake of the strut, however, is a significant function of the test speed, driving deeper with increasing speed.

Following the inception of cavitation on the strut, a growing region of cavitation develops. For these struts and yaw angles the cavitating region coalesces into one cavity with a generally steady shape, which is periodically

disrupted by reentrant flow from the rear end or the sides of the cavity. The spanwise distribution of the cavity length is a function of the aspect ratio, the existence of end plates or other structures, and the Froude number. The upper edge of the cavity is influenced by the proximity of the nearby free-surface. The shape of the cavity wall and the water surface is shown for typical cases in the photographs of figures 9 and 10, and in the diagrams of figures 11 and 12. Also included in the latter figures are the water profiles which were observed in noncavitating flow. It is observed that the rear portion of the upper edge of the cavity moves upward as the cavitation number is reduced. The water surface is noted to have moved upward more slowly than the cavity wall. If these two surfaces continued at these rates they would ultimately intersect, and ventilation could be expected. However, there are other features in the flow which intercede.

Large disturbances (up to ½-inch diameter) are seen to protrude below the mean surface of the drawn-down water. These have been referred to as Rankine vortices[3]. Analysis of these photos and the excellent photos of Reference 8 has revealed that these disturbances grow rapidly in length and width as they move relative to the strut. Extrapolating toward the leading edge from the region where the diameter of these disturbances can be measured, the probable size of the initial disturbance is on the order of the thickness of the boundary layer. Hence, it is concluded that the vorticity shed from the boundary layer is the probable source for the initial disturbance of the water surface. The rapid growth of these small disturbances is a result of the large acceleration (up to 20G) which the free surface experiences as it is drawn down while passing the strut. The instability of the accelerated interface between a liquid and air, known as the Taylor instability[10], has been studied[11] for finite disturbances and large growth, as exist in this problem. Photographs of this phenomenon presented in reference 11 appear to be identical with those obtained[8] with the strut models just prior to ventilation inception. While these growing disturbances appear to provide a mechanism for penetrating into the vapor cavity, computations of their rate of growth indicates that there is insufficient time for these disturbances to

penetrate into the cavity under conditions for which ventilation occurs. Further evaluation of the flow data reveal that under some circumstances, thin vortex cores extend at great speed from the bottom of these longer disturbances. Figure 1: illustrates this ventilation mechanism. There are two probable sources for strong vortex flow adjacent to the strut. These are the original boundary layer vorticity and the highly rotational flow which exists over the top edge of the vapor cavity as the flow forms the spray sheet on the inside of the cavity[9]. Penetration of one of these vortex cores into the cavity while it passes the strut would allow moderate step-like increases (10 to 20% per vortex) in the cavity pressure. Such pressure jumps would have noticeable effects on the cavity shape.

There are two other possible mechanisms for inception of ventilation which should not be overlooked. The extensive reentrant flow into the cavities from both the rear and the upper and lower edges of the cavity cause significant disturbances to the overall cavitation pattern. As portions of this erratic, internal flow encounter the otherwise stable walls of the cavity, either at the leading edge or the upper edge, major transient changes in the flow around the cavity are developed. These lead to the periodic shedding and the large force oscillations usually reported for cavities having lengths which are between 0.6 and 1.5 chord lengths. Ventilation inception for several of the test conditions reported herein was initiated by the blasting of this erratic, internal flow through the thin sheet of water between the cavity and the free surface. The disturbance caused by this jet undoubtedly allowed air-flow passages to be developed in a different manner than hypothesized previously. The test conditions for ventilation resulting from this type of jet action were undistinguishable from the rest of the data. The other possible ventilation mechanism is that resulting from unsteady oscillations of the pressure in the vapor cavity as caused by shedding and reentrant flow disturbances. Since there were no pressure measurements obtained within the strut cavities, it is not possible to thoroughly evaluate the significance of this ventilation mechanism. It can be estimated that the shedding of cavities by reentrant flow would produce pressure oscillations having a maximum frequency of $\frac{1}{10}\frac{V}{c}$ (Ref. 16) or 3 cps at 30 fps. In contrast, the undulations in the cavity wall

during transition to ventilation are characterized by a frequency of approximately 50 cps. This difference relegates the cavity pressure oscillation (if it exists) to the role of a forcing function which tends to promote ventilation rather than to the role of the actual inception mechanism.

The typical ventilation transition event shown in figure 7 has several features which support the hypothesized inception mechanism. The first indication of inception of ventilation is the sudden change in the shape of the cavity between the leading edge and the mid chord (frame 3). In the next frame the disturbed cavity is propagated along the strut by 0.33 chords of travel. However, no new disturbance of the front portion of the cavity occurs, indicating that there are no further changes in the cavity pressure. In the next frame (5) the cavity edge near the leading edge of the strut is observed to move again and to continue to move up the strut during subsequent frames. This second jump is undoubtedly caused by the pressure rise resulting from the penetration of more vortex cores into the previously displaced cavity wall. As late as frame 7 there appears to be a single, unified, rapidly growing cavity which extends well up and under the spray sheet. The maximum length of the cavity is seen to have doubled in 5 frames (0.05 seconds=1.5 chords of travel). Measurements of the cavity length, the elevation of the cavity at the quarter chord line, and the percentage change in the side force are shown in figure 14. The simultaneity of the flow changes indicates that the ventilation mechanism is predominately a process of changing the cavitation pattern from a small vapor-filled cavity to one large, air-filled cavity by way of a straightforward air in-flow process. The hesitation in the cavity elevation as shown in this figure is quite typical, with some tests encountering as many as 4 to 6 distinct oscillations during the transition phase. The occurrence of these step-wise motions lends support to the ventilation mechanism based on multiple vortex core penetrations. It is significant to note that the maximum rate of growth in cavity length is equivalent to the test speed. This means that the strut is simply extending the cavity which was previously created.

The force records were examined to indicate factors which influence the time (or rate) of the ventilation transition. Tests at 20, 25, and 30 fps for yaw angles of -8 degrees were found to require approximately 0.07 seconds for the

principal change in force to occur (excluding the transients). This represents travel distances of 1.4 to 2.1 feet. The transition time was noted to vary inversely with the yaw angle and to be insensitive to submergence or nose radius.

This section has reviewed the results of the tests conducted in LUMF and as augmented by data from NSRDC to develop an understanding of the process of ventilation of a cavitating strut. From this development it is concluded that the parameters which influence cavity size and shape are undoubtedly the most significant parameters that need to be evaluated with regard to the conditions for inception of ventilation.

7.2 Conditions for Inception of Ventilation

The knowledge of the conditions under which surface ventilation occurs is crucial to the selection of configurations to avoid ventilation, as well as to an understanding of the mechanism which produces ventilation. The latter may ultimately lead to more effective solution of the former. A review of the test film and the oscillograms showed that there were two methods which could be used to define the inception of ventilation. The sudden change in the side force records was very distinct and allowed convenient determination from the test record of the test speed and forces at the time of inception. The data film showed similar radical changes in the flow, but required reference to the oscillogram for ultimate determination of the conditions at inception. A comparison of results, as in figure 14, indicated the validity of utilizing the break in the force records as an accurate identification of the conditions for inception.

Figures 15 through 21 present these conditions for ventilation inception in the form of the vapor cavitation number at the water surface as function of the carriage speed for the several models, yaw angles, and submergence ratios. The solid symbols identify the conditions for which natural ventilation inception occurred, while the open symbols indicate test conditions for which ventilation was not obtained. The narrow lines indicate the approximate range

of conditions which were encountered during the slowly accelerating portion of the test run. The broad lines extending to higher speeds than the inception condition indicate the conditions under which the strut continued to ventilate as the constant speed portion of the test run was approached. The symbols without lines represent test runs which were made at constant conditions, following catapulting of the towing carriage to speed. Included for comparison are the ventilation inception conditions for the struts as tested at NSRDC[12] including some extrapolated conditions.

It is seen in these figures that the vapor cavitation number at the water surface for incipient ventilation is nearly independent of the testing speed. This means that surface ventilation in the presence of cavitation is predominantly influenced by the cavitation (cavity length, location, or stability). The effects of fluid inertia, viscosity, and surface tension for a model of this size are apparently nominal. The incipient cavitation numbers for the LUMF data (at moderate speeds) are equal to or less than those obtained at NSRDC (at high speeds). It is of interest to note that even smaller variations in vapor cavitation number for incipient ventilation are obtained if the cavitation number is based on the pressure at a more representative depth below the surface. Observation of the cavity shapes at conditions incipient to ventilation suggested that a depth of 0.1 chord lengths would be representative for the strut model 2 at -8 degrees yaw angle. Figure 22 represents the test conditions for this model based on a vapor cavitation number for a depth of 0.1 chord lengths. Although the change in results is not large, it is quite evident that a better correlation is provided over a wide range of test speeds. The importance of this better correlation is that it reduces the number of parameters which must be considered as being relevant to the mechanism of ventilation. On the other hand, the effective use of this representative cavitation number requires that there be sufficient data available to predict the depth to be used in the computation of cavitation numbers. The limited amount of pertinent data and its significant scatter restrict the assessment of representative depths to a recognition of trends which are substantiated by the data shown in figures 15-21. These trends are that more correction (greater representative

depth) is required for the struts with smaller nose radii and for the struts which are operated at larger yaw angles. Blunt struts at small angles require no correction for good correlation.

The effect of yaw angle on the surface vapor cavitation number for ventilation inception is illustrated in figure 23. The cavitation number for ventilation is seen to increase with increasing yaw angle at more than a linear rate. A significantly lower cavitation number is required for ventilation of the circular arc section (model 0) at -8 degrees. However, the advantage seems to be lost as the yaw angle exceeds -10 degrees. The strut with the largest nose radius (model 3) in all cases ventilates at higher cavitation numbers than the other struts.

This evaluation of the conditions necessary for ventilation inception has concluded that cavitation is the most significant feature in the flow field which leads to surface ventilation. Accurate representation of the cavitating conditions apparently requires some form of consideration of a representative depth. The importance of these conclusions is that scale-model testing for ventilation inception principally requires scaling of the vapor cavitation number, while scaling of the Froude number would automatically provide the correction for a representative depth. Corrections for the Froude number effect may be negligible (blunt strut at moderate yaw angles) or may require separate determination. Model tests at inordinately high Froude numbers apparently provide conservative inception conditions.

The next section of this discussion presents the measured force data in both ventilating and non-ventilating conditions.

7.3 Measured Forces

The side force and drag force coefficients obtained for strut models 0, 2, and 3 are presented in figures 24 through 30 as functions of the vapor cavitation number at the surface of the water. In these figures the forces which were measured under ventilating conditions are indicated by a solid symbol, while those tests in which artificial ventilation was attempted by blowing air at the start of the test run are indicated by a flagged symbol.

The strut force characteristics with partial cavitation are similar to those customarily encountered with fully submerged hydrofoil section. The side force coefficients do not change significantly when cavitation is initially encountered. At lower cavitation numbers the larger cavities produce significantly larger side forces when the struts are at yaw angles of -8 and -10 degrees. At -6 degrees the side force coefficient remains essentially constant throughout the cavitating range. This variable effect of cavitation is readily explained. The changes in the pressure distributions caused by cavitation at small incidence angles are small and hence there are small changes in the forces. The change in the pressure distribution is greatly increased as the angle of incidence is increased, causing a larger low pressure region to occur, thereby increasing the normal force. The erratic nature of the side force data near ventilation is partially indicative of the large variations in forces which occur as major portions of the cavity are periodically shed. An added cause for the force scatter was observed during several runs in which there was some form of cavitation on the "pressure" side of the strut model. This was evidenced by changes in the cavity shape behind the trailing edge of the strut which were not related to events occurring on the low pressure side of the strut. The variable occurrence of cavitation on the pressure surface will also have a significant effect on the scatter in the side force measurements. Photographs[8] of the pressure side of these struts show distinct areas of cavitation beyond the mid-chord of the strut in the region of ventilation inception. The arrangement of cameras and lights for this test program, unfortunately, precluded direct observation of the pressure side of the strut. However, it is quite evident that the local pressures on the "pressure" surface of the strut will readily approach vapor pressure for the small angles of incidence tested and for these relatively thick (12%) struts.

The drag force, also, increases in magnitude as the cavitation number is reduced. This increase occurs for all the strut models and at all the tested yaw angles. This result again is similar to that observed with submerged hydrofoil sections.

Drastic sideforce reversals occur when ventilation of the strut has been established. It is this well document[1-3] characteristic which has led to these studies. The reduced scatter in the side force coefficient is a result of the

steady-state flow condition existing with the large, full cavity on the low pressure side of the strut and the generally higher pressure field which exists on the "pressure" surface, which eliminates the potential for vapor cavitation on the pressure surface. Since these two effects should provide extremely stable flow conditions and highly repeatable force measurements, it is apparent from the remaining scatter of the force data that transient phenomena were still influencing the test data as obtained. A review of the test oscillograms revealed that the side forces on the strut models experienced significant transients following the major force change. Because of the limited run time for these tests it was not always possible to wait out the decay or even to obtain measurements at a constant time after ventilation transition occurred. It is simply concluded that the observed scatter in measured forces is somewhat a measure of the magnitude of the time-dependent transient forces which accompany ventilation transition.

The constant value of both the side force and drag force for the artificially (blowing) ventilated conditions, which is the same as their value in the naturally ventilating conditions, provides firm evidence that the flow field is essentially under a zero cavitation number condition for these constant Froude number tests. Empirical evaluation[3] of ventilated side force coefficients over a range of speeds has shown a predictable Froude number effect.

The average side force coefficients for the fully-wetted condition and for the fully-ventilated condition at 30 fps and a submergence of 1 chord length are presented in figure 31 as a function of the yaw angle. The general characteristics of these data in fully wetted flow are as expected. Comparison of the data point at -8 degrees for the circular arc model (0) with those obtained at SIT[3] shows essentially the same side force coefficient for the 1-foot chord model in LUMF as for the ¼-foot chord model at SIT. The sudden shifts in the wetted side force coefficients for models 2 and 3 between -6 and -8 degrees is assumed to be caused by laminar boundary layer separation near the leading edge of the strut. This phenomena has been extensively reviewed[15] for airfoil sections in similar ranges of Reynolds numbers. The effect of the small aspect ratio of these struts on the boundary layer separation has not been studied in detail. Some flow visualization observations[3], have

indicated typical separation regions during tests at lower Reynolds numbers.

Theoretical side force coefficients in wetted flow, which were presented in Reference 3, have been plotted in figure 31 for comparison with the test results. The value of the Weissinger, L-method is apparent for the smaller nose radius and for conditions for which the boundary layer can be expected to separate from near the leading edge of the strut. The lifting line theory is obviously inadequate for representing the force coefficient for these small aspect ratios. The data presented in Reference 3 indicates improved comparison with this theory for an aspect ratio of 2:1.

Side forces in the fully ventilated condition increase in magnitude as the yaw angle is reduced. Again these results are in general agreement with both the experimental data and the theoretical trends as reported by SIT[3]. It is of interest to note that the ventilated side force increases with increasing nose radius. This result suggests that a strut having a minimal nose radius would have the least undesireable effects, if ventilation were encountered.

8. CONCLUSIONS AND RECOMMENDATIONS

The following conclusions have been developed in the course of this study.

Mechanism of Ventilation Inception

1. The displacement of the water surface adjacent tothe strut during the passage of a non-cavitating strut is independent of forward speed.
2. The wake behind a non-cavitating strut is function of the speed (or Froude number).
3. The water surface displacement is altered by the presence of a vapor cavity.
4. The most commonly occurring and most probable mechanism causing the inception of ventilation is the penetration into the vapor cavity of small vortex cores developed from large disturbances on the surface of the water which grow by Taylor instability from small disturbances which may be a result of shed vorticity from the strut boundary layer.

5. The transition from incipience to full ventilation occurs with distinct oscillations in the flow pattern but with smooth changes in cavity length and the overall forces.

6. The time for the major effects of ventilation to take place was approximately 0.07 seconds at a yaw angle of -8 degrees. The time varied inversely with yaw angle and was insensitive to nose radius or submergence.

7. Several tests were observed to experience ventilation inception as a result of penetration of the water sheet by erratic reentrant-jet flow from inside the vapor cavity.

Conditions for Inception of Ventilation

1. The vapor cavitation number is the mostsignificant parameter influencing ventilation inception.

2. Selection of a representative depth for determining the vapor cavitation number provided an improved comparison between the NSRDC data attained at high speed and the LUMF data obtained at moderate speeds. A depth of 0.1 chord lengths was effective in improving the comparison for strut model 2 at a yaw angle of -8 degrees. (The use of a representative depth for improved comparison of results is in effect a Froude number correction.)

3. The cavitation number required for inception of ventilation was a direct function of the radius of the leading edge of the strut models in the range of angles from -6 to -10 degrees.

Measured Forces

1. The forces on the strut models increased as the amount of cavitation was increased for large yaw angles and remained unchanged for a yaw angle of -6 degrees.

2. The side force reversed direction upon full ventilation of the strut models for yaw angles from -6 to -10 degrees.

3. The side force developed by artificially induced ventilation (by blowing air) was independent of the ambient pressure in the tank

indicating a condition of essentially zero cavitation number.

4. The side force developed during ventilation conditions was a direct function of the radius of the leading edge of the strut model.

5. The side force measured on the circular arc strut model (0) compared well with data from SIT[3].

The following recommendations have been developed during this study.

1. The distinct advantages shown by the circular arc strut model (low vapor cavitation number for inception and low force reversal if ventilation occurs) suggest that further work on strut ventilation should be directed to this class of sections.

2. The effect of Froude number, only suggested in the current study as a means of providing a small improvement in data comparison, should be examined more closely with wider ranges of speeds and models sizes.

3. Scale-model testing of surface piercing struts can be adequately (if not preferably) performed at moderate speeds under conditions of variable, vapor cavitation number.

9. REFERENCES

1. Wadlin, K. L., "Mechanism of Ventilation Inception," Second Symposium, Naval Hydrodynamics, ONR/ACR-38, Aug. 1958.

2. Barr, R. A., "Ventilation Inception of Surface Piercing and Submerged Foils and Struts, Chapter 3 of Hydrodynamics of Hydrofoil Craft, Subcavitating Hydrofoil System," Hydronautics, Inc., Technical Report 463-1.

3. Breslin, J. P. and Skalak, R., "Exploratory Study of Ventilated Flows About Yawed Surface Piercing Struts," National Aeronautics and Space Administration, Memo 2-23-59W, April 1959.

4. Waid, R. L., "Cavitation Research Capabilities of the Lockheed Underwater Missile Facility," Symposium on Cavitation Research Facilities and Techniques, American Society of Mechanical Engineers, 1964.

5. Wetzel, J. M., "Ventilation of Bodies Piercing a Free Surface," Second Symposium, Naval Hydrodynamics, ONR/ACR-38, 1964.

6. "Hydrodynamic Characteristics of a Base-Vented and Supercavitating Strut for Hydrofoil Ships," Aerojet-General Corp., Report No. 2796, August 1964.

7. "Waterjet Propulsion System Study, Report No. 4, External Flow Tests," Lockheed California Company, LR 17885-4.

8. Rothblum, R. S., and Wilburn, G. M., "Investigation of Ventilation of Surface Piercing Struts," Naval Ship Research and Development Center, Test and Evaluation Report 217-H-01, June 1967.

9. Waid, R. L., "Experimental Investigation of the BuShips Parent Hydrofoil--Lockheed Underwater Missile Facility," Lockheed Missiles & Space Company, LMSC/805568, December 1965.

10. Taylor, G. I., "The Instability of Liquid Surfaces When Accelerated in a Direction Perpendicular to Their Planes," Proc. Roy. Soc. A, 201, 192-6, 1950.

11. Emmons, H. W., Chang, C. T., and Watson, B. D., "Taylor Instability of Finite Surface Waves," Jour. of Fluid Mech., Vol. 7, Part 2, Feb. 1960.

12. Mayer, D. A., "Investigation of Surface Piercing Struts," Naval Ship Research and Development Center, Report (in preparation 1968).

13. Kiceniuck, T., "A Preliminary Experimental Study of Vertical Hydrofoils of Low Aspect Ratio Piercing a Water Surface," California Institute of Technology, Hydrodynamics Laboratory, Report No. E-55.2, December 1954.

14. Chey, Y., and Kowalski, T., "Interference Effects of a Submerged Hydrofoil on a Surface-Piercing Strut," Stevens Institute of Technology, Davidson Laboratory, Report 936, June 1963.

15. McCullough, G. B., and Gault, D. E., "Examples of Three Representative Types of Airfoil-Section Stall at Low Speeds," NACA TN 2502, Sept., 1951.

16. Wade, R. B., and Acosta, A. J., "Experimental Observation on the Flow Past a Plano-Convex Hydrofoil," California Institute of Technology, Hydrodynamics Laboratory, Report No. E-79.8, Feb. 1965.

TABLE I

COORDINATES OF LEADING EDGE OF STRUT MODELS

Dist. from Leading Edge In.	Distance from Strut Centerline - in.		
	STRUT 1	STRUT 2	STRUT 3
0	0	0	0
.030	.082	.107	.140
.060	.113	.146	.191
.090	.136	.175	.227
.120	.155	.198	.255
.180	.186	.234	.299
.240	.211	.263	.332
.300	.232	.286	.359
.360	.250	.306	.380
.480	.282	.339	.416
.600	.308	.366	.443
.720	.331	.388	.464
.840	.352	.408	.482
.960	.371	.425	.496
1.080	.389	.440	.508
1.200	.405	.454	.519
1.320	.420	.467	.529
1.440	.435	.479	.537
1.560	.449	.490	.545
1.680	.462	.501	.552
1.800	.475	.511	.559
1.920	.487	.521	.565
2.100	.505	.535	.574
2.400	.533	.557	.589
2.700	.559	.578	.603
3.000	.584	.598	.618
3.300	.607	.618	.632
3.600	.628	.636	.646
3.900	.648	.653	.660
4.200	.666	.669	.673
4.500	.681	.683	.686
4.800	.694	.695	.697
5.100	.705	.706	.706
5.400	.713	.713	.714
5.700	.718	.718	.718
6.000	.720	.720	.720
NOSE RADIUS - in.	.122	.219	.392
NOSE RADIUS/CHORD	.0102	.0182	.0327

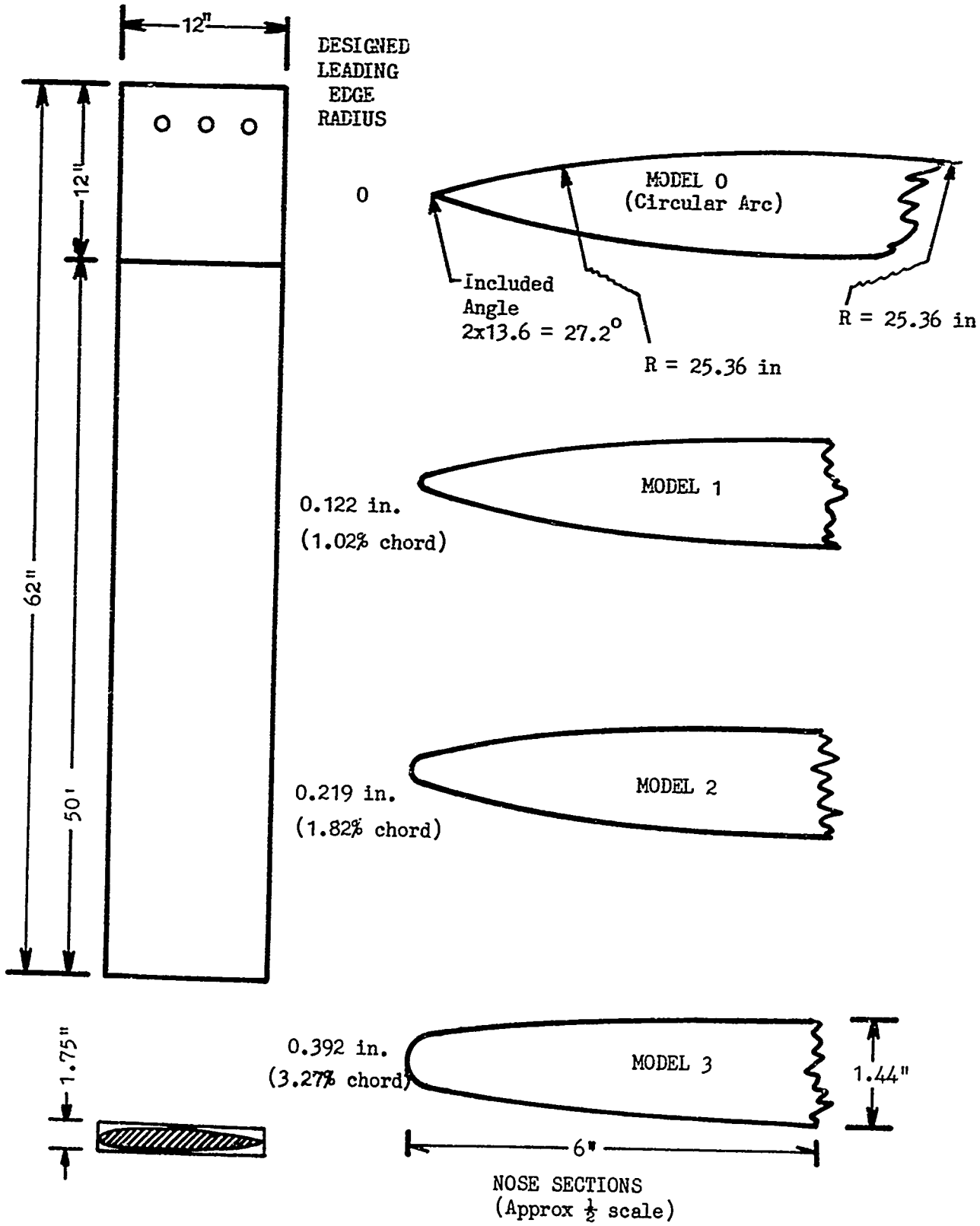

Figure 1. Physical Characteristics of Strut Models

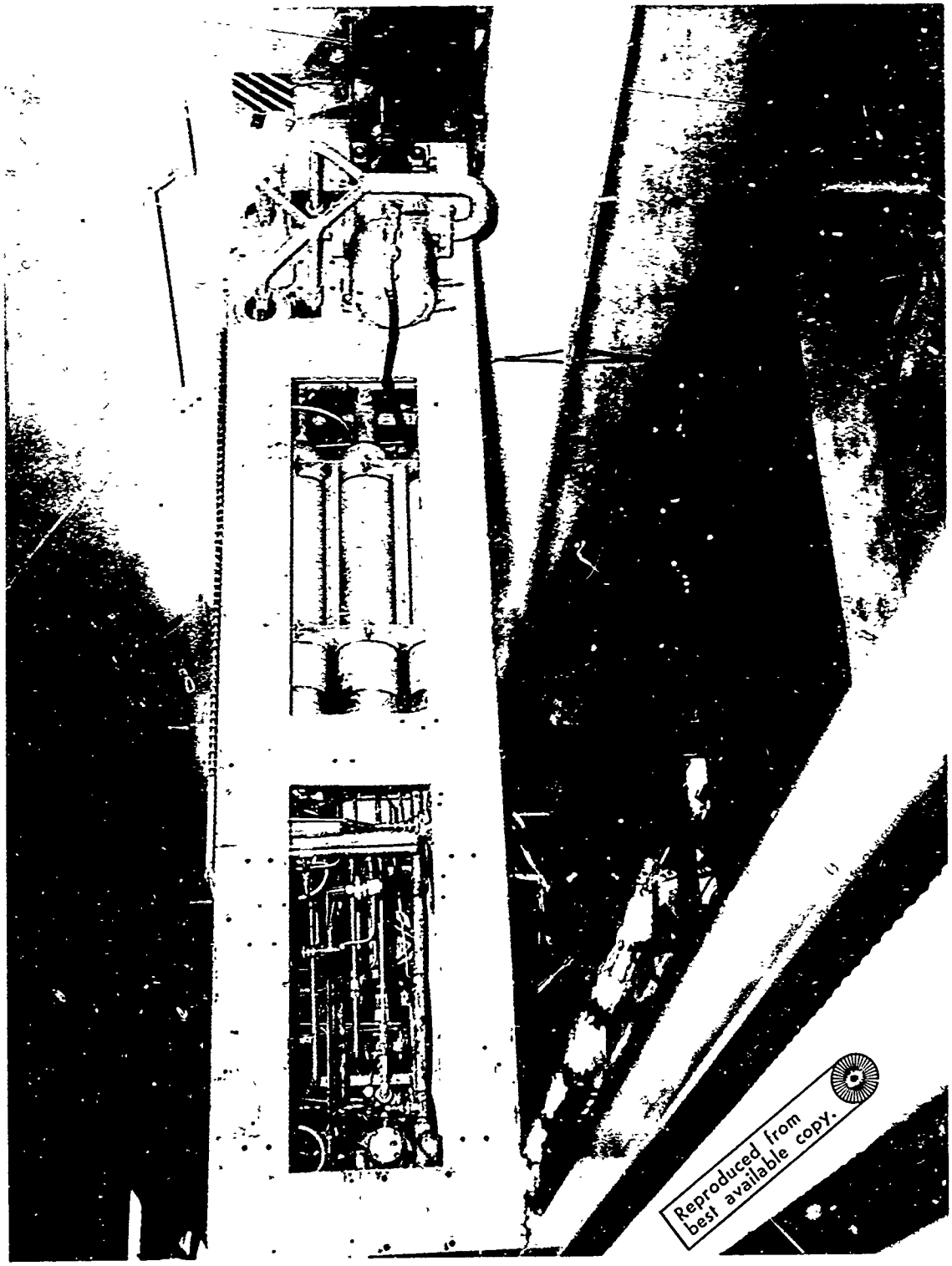

Reproduced from best available copy.

FIGURE 2. Photograph of Towing Carriage with Strut Model Installed

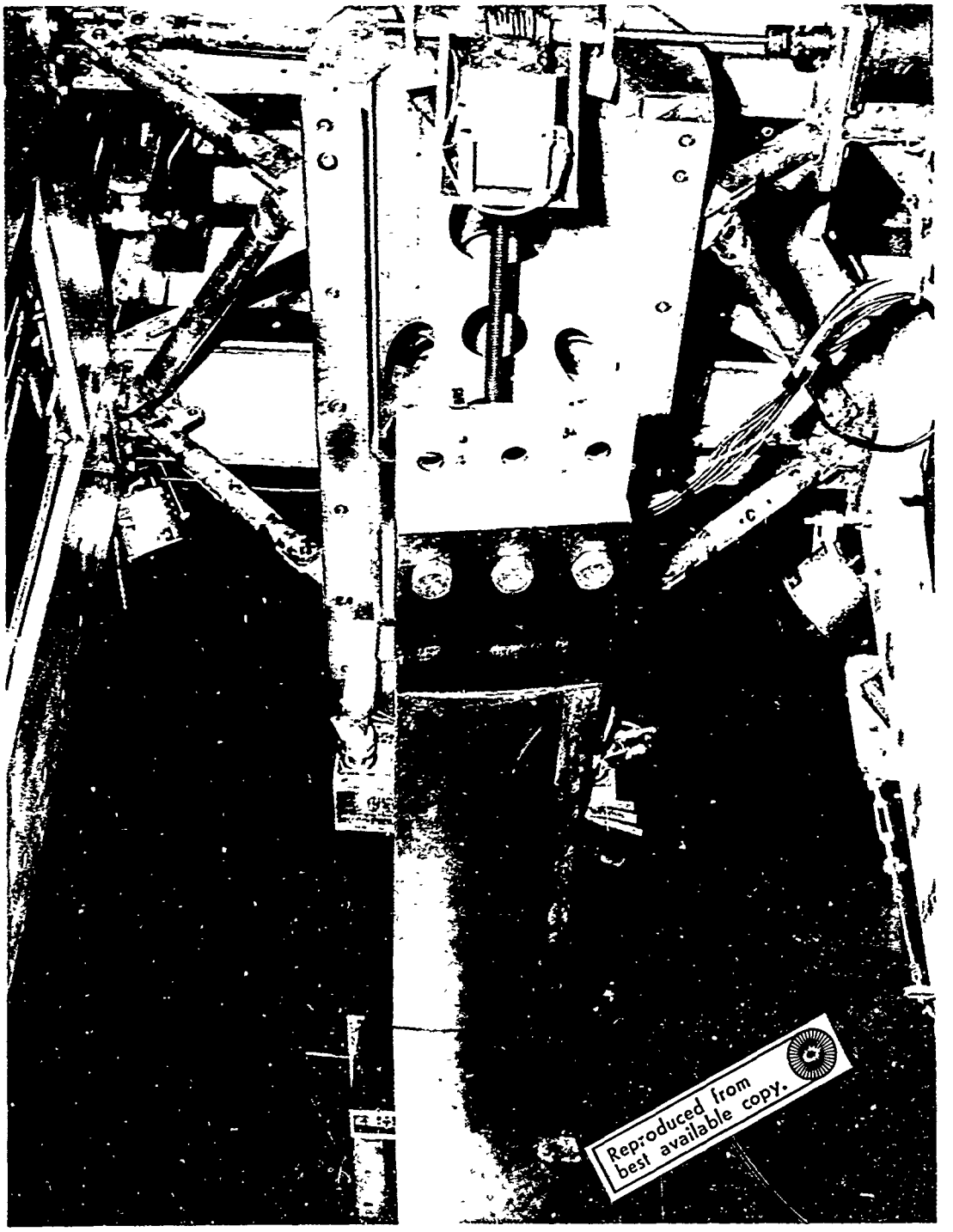

FIGURE 3. Photograph of strut model installation on force balance and elevating mechanism

FIGURE 4. Cavitation on Strut Model O at a Yaw Angle of -8 Degrees

FIGURE 5. Inception of Ventilation on Strut Model O at a Yaw Angle of -8 Degrees

FIGURE 6. Fully Developed Ventilation on Strut Model O at a Yaw Angle of -8 Degrees

Reproduced from best available copy.

FIGURE 7. Strip of motion picture film showing ventilation inception and transition for strut model 2 at a yaw angle of -8 degrees and a speed of 30 fps. (time between successive frames was 0.01 seconds)

Reproduced from best available copy.

FIGURE 7. (Continued)

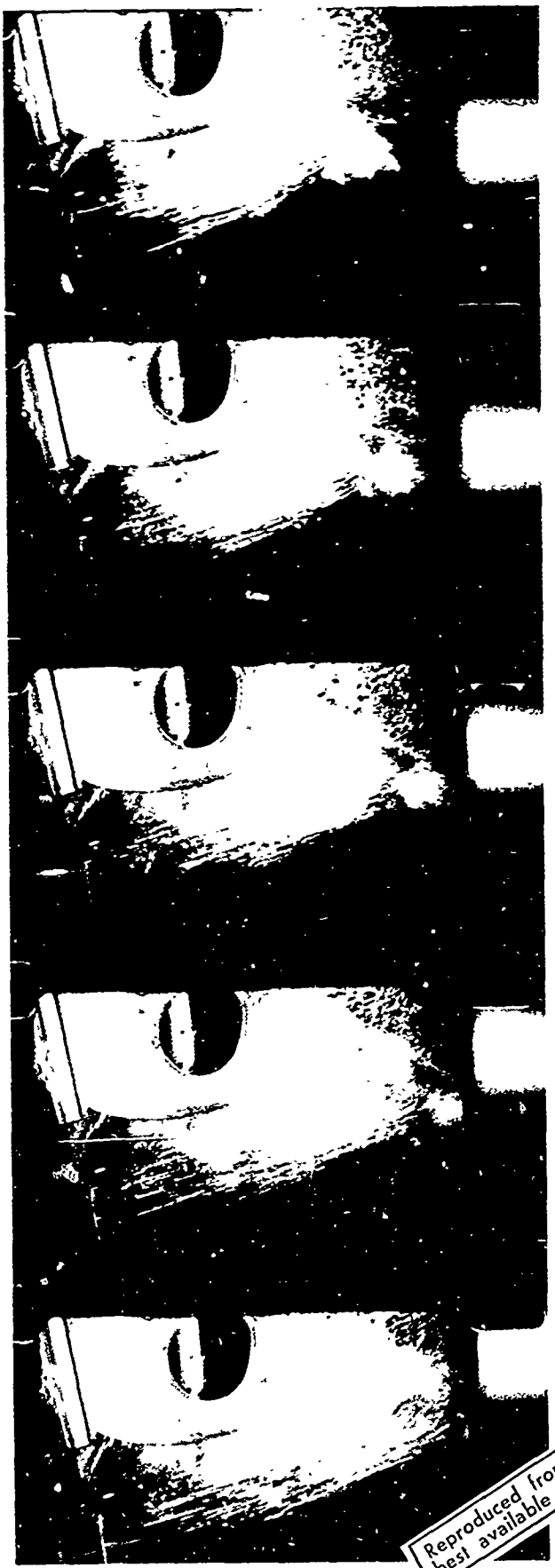

Reproduced from best available copy.

FIGURE 7. (Continued)

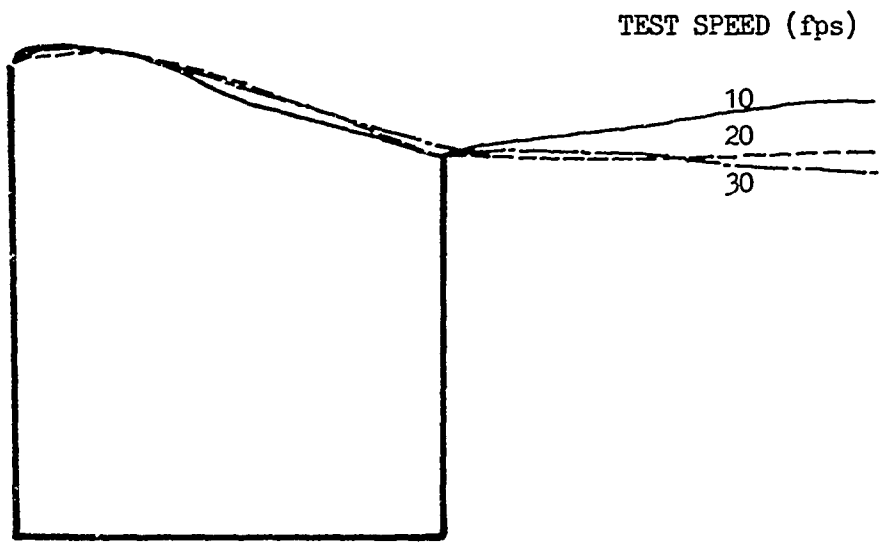

FIGURE 8. Elevation of the surface of the water adjacent to strut model at a yaw angle of -10 degrees for noncavitating conditions.

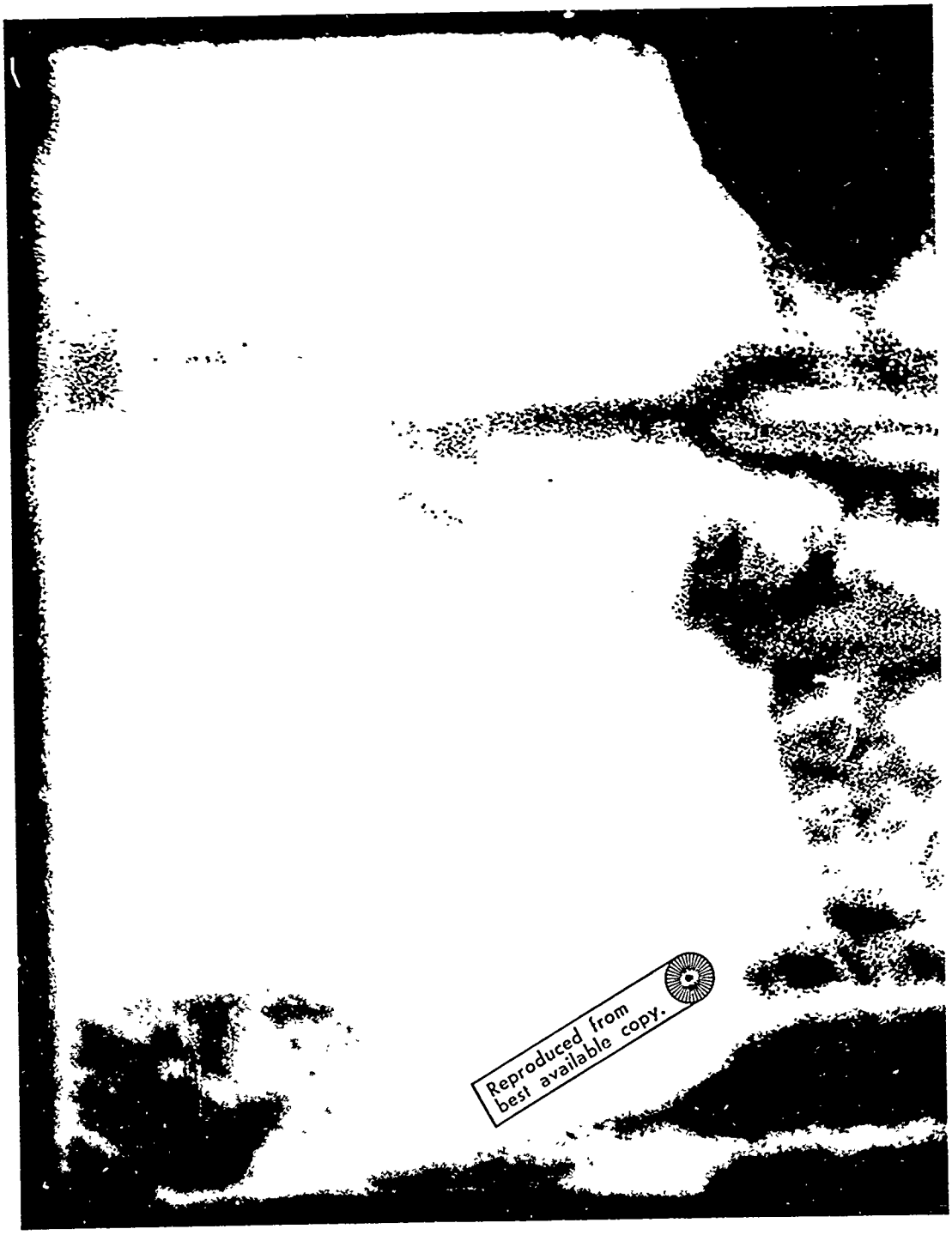

FIGURE 9. Underwater Photograph of Strut Model 0 at a Yaw Angle of -8 Degrees

FIGURE 10. Underwater Photograph of Strut Model 3 at Yaw Angle of -6 Degrees

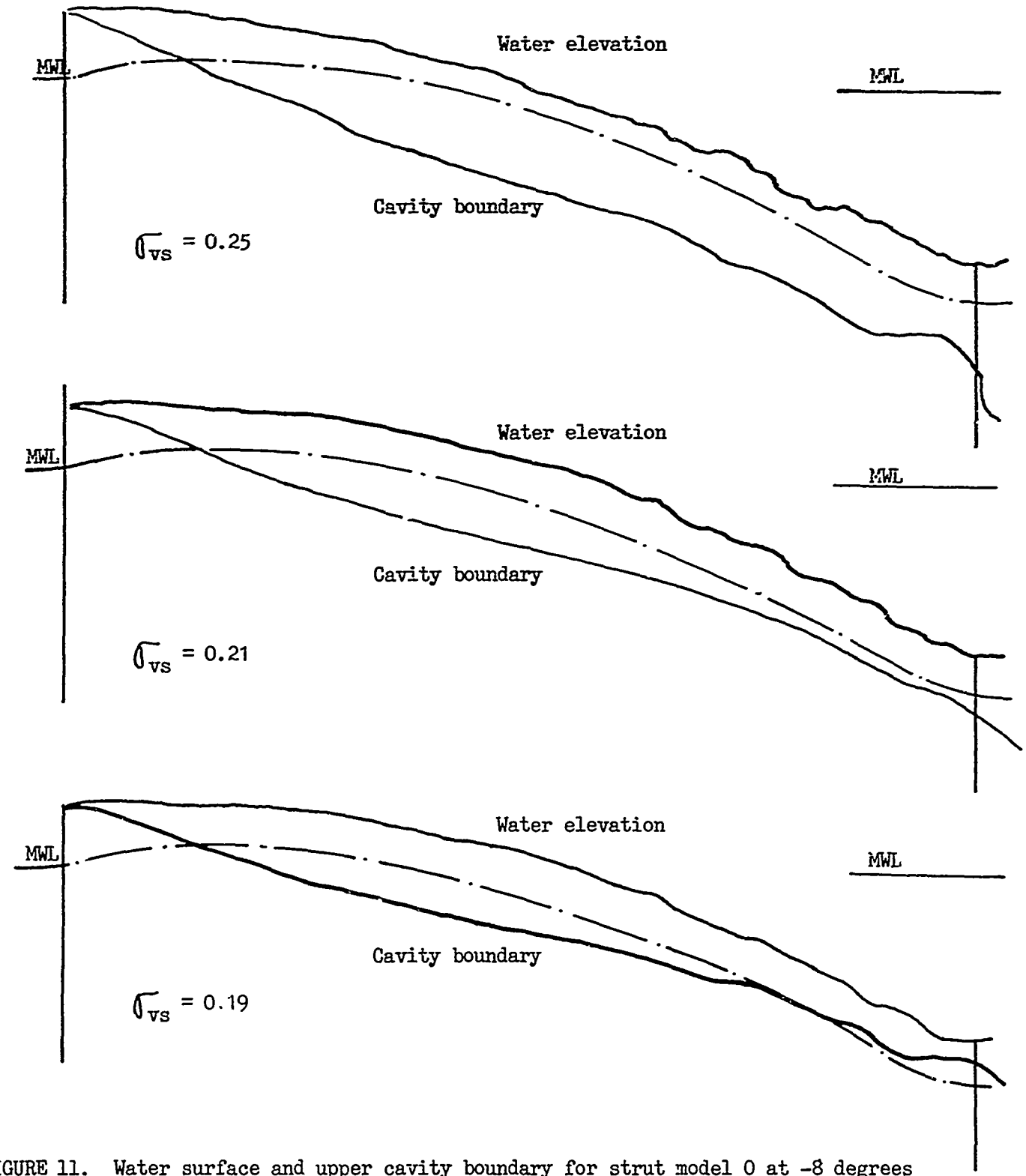

FIGURE 11. Water surface and upper cavity boundary for strut model 0 at -8 degrees yaw angle for a speed of 30 fps. (Water surface elevation with no cavitation is shown for reference).

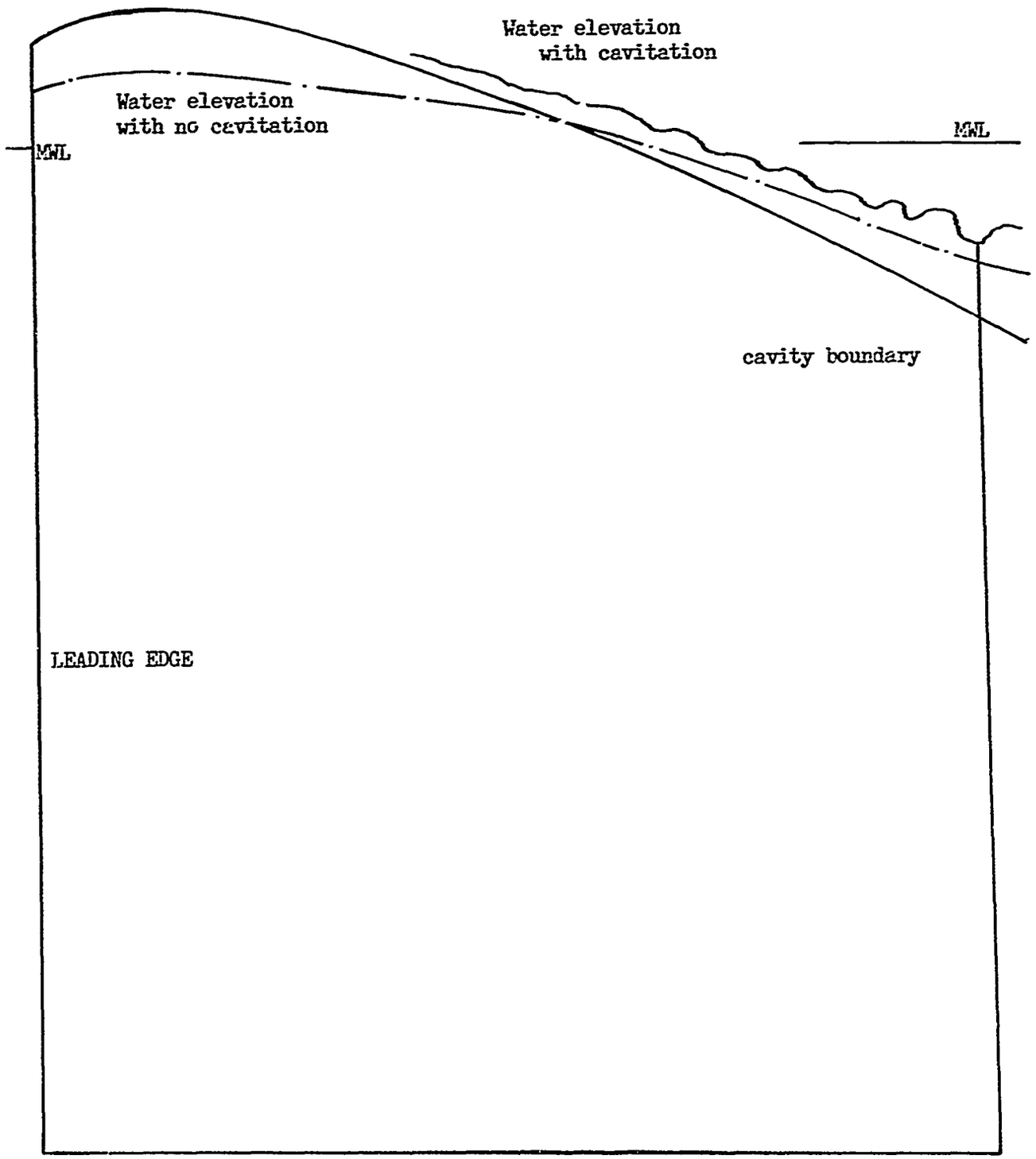

FIGURE 12. Water surface and upper cavity boundary for strut model 3 at -6 degrees yaw angle for a speed of 30 fps and a surface vapor cavitation number of 0.24.

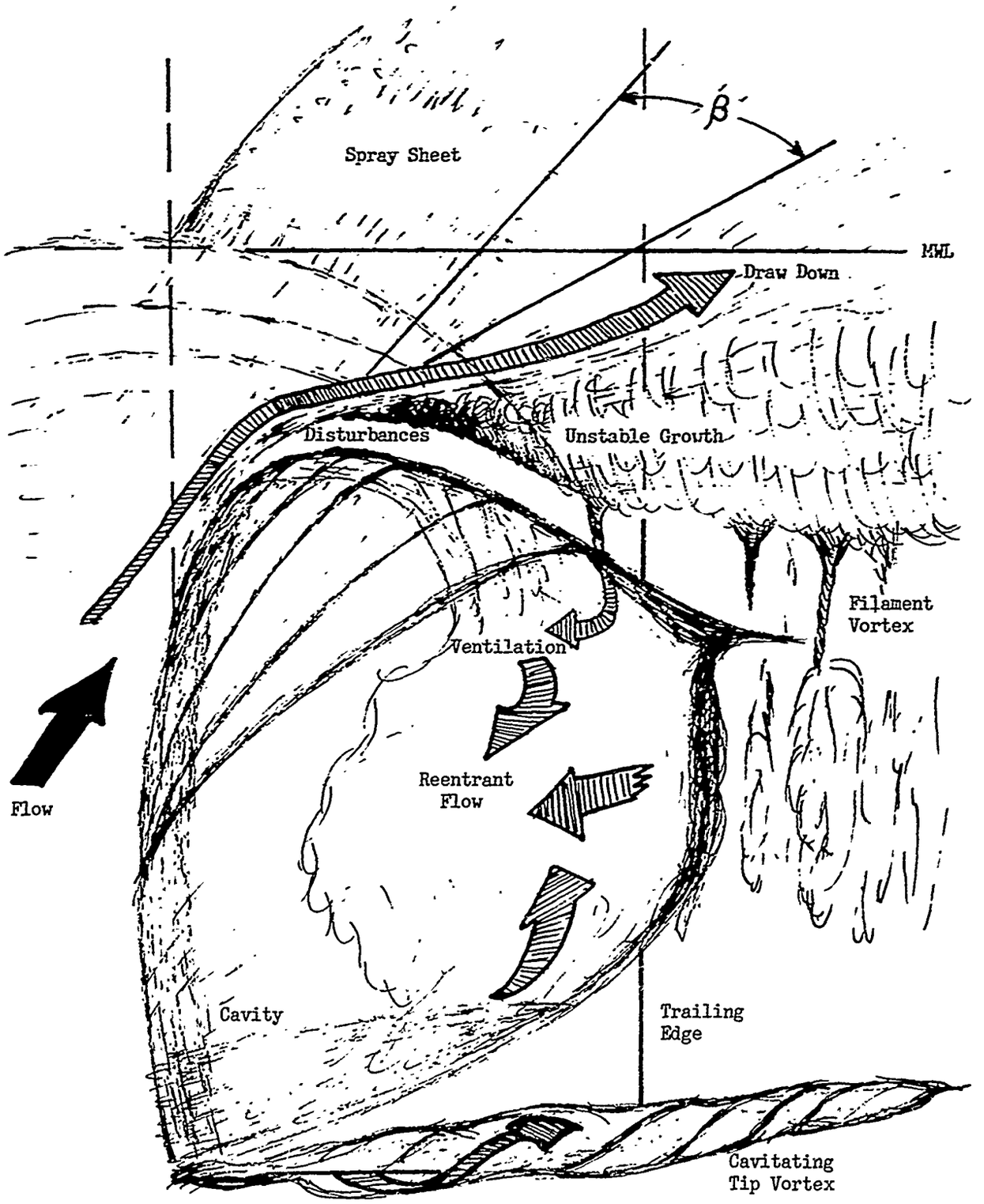

FIGURE 13. Sketch of mechanism for inception of surface ventilation of a yawed strut through filament-like vortex cores.

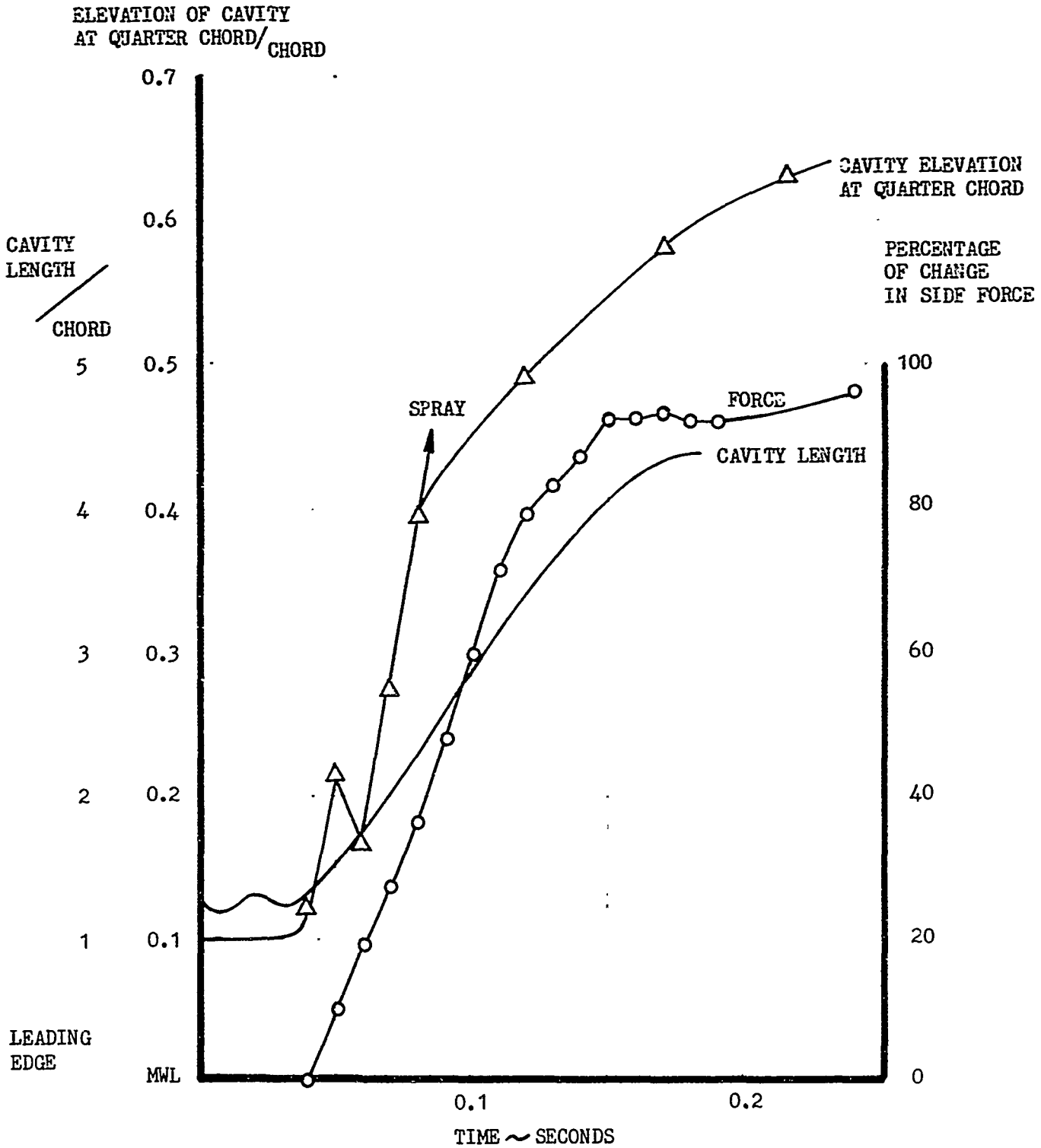

FIGURE 14. Force and cavitation characteristics during ventilation transition of strut model 2 at a yaw angle of -8 degrees for a speed of 30 fps and a surface vapor cavitation number of 0.293

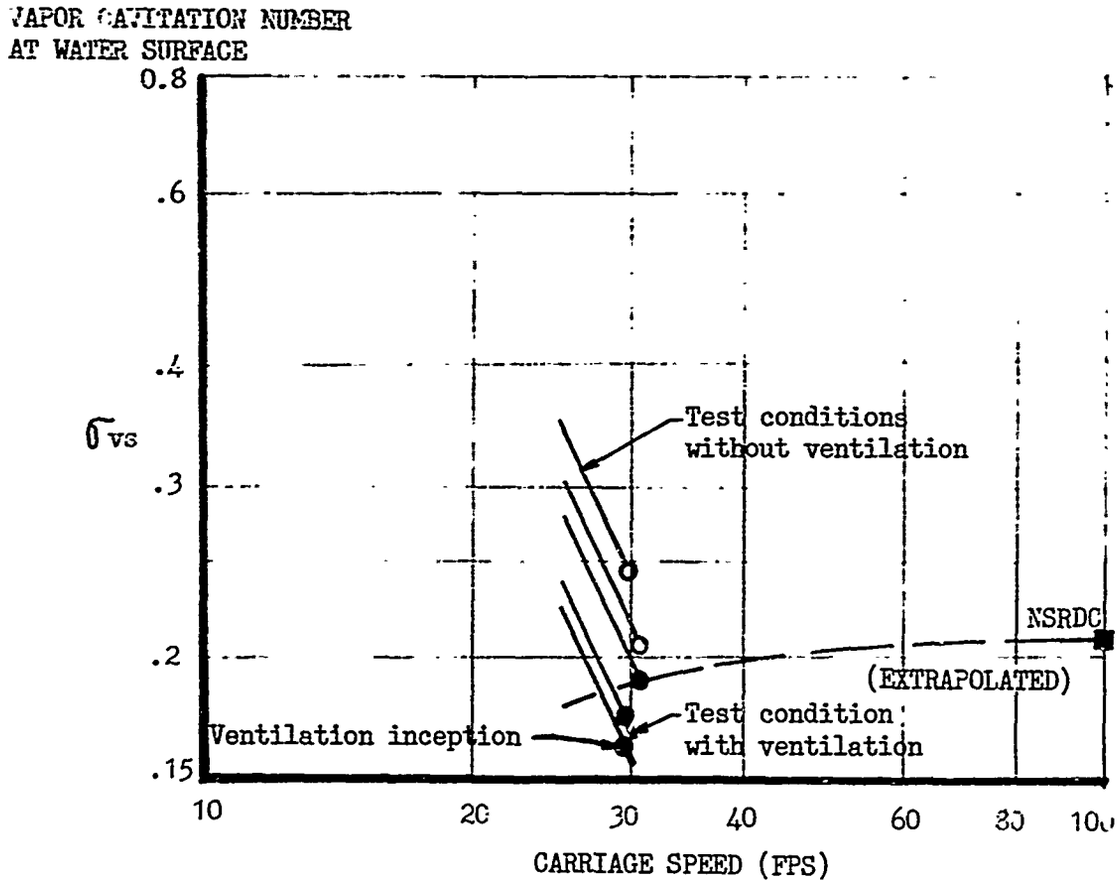

FIGURE 15. Conditions of flow for strut model 0 at a yaw angle of -8 degrees and a submergence of 1.0 chords. (Solid symbol indicates ventilation.)

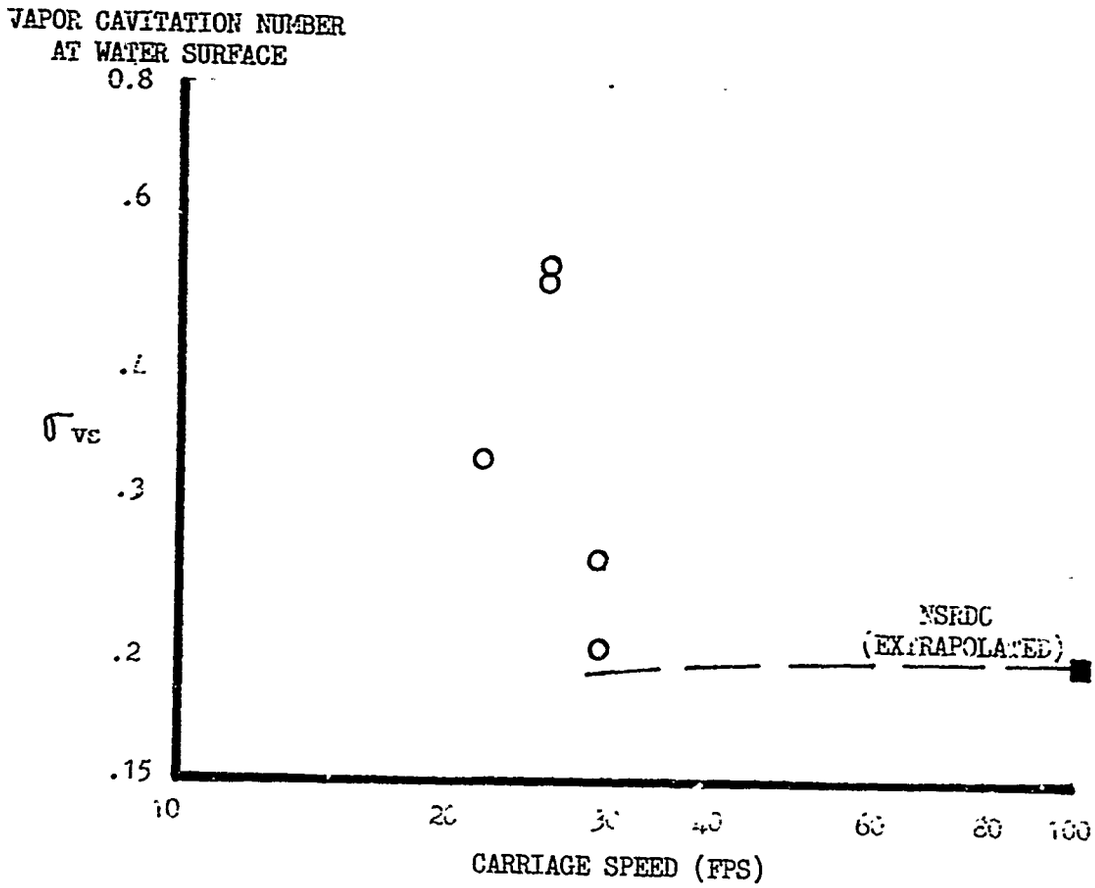

FIGURE 16. Conditions of flow for strut model 2 at a yaw angle of -6 degrees and a submergence of 1.0 chords. (Solid symbol indicates ventilation).

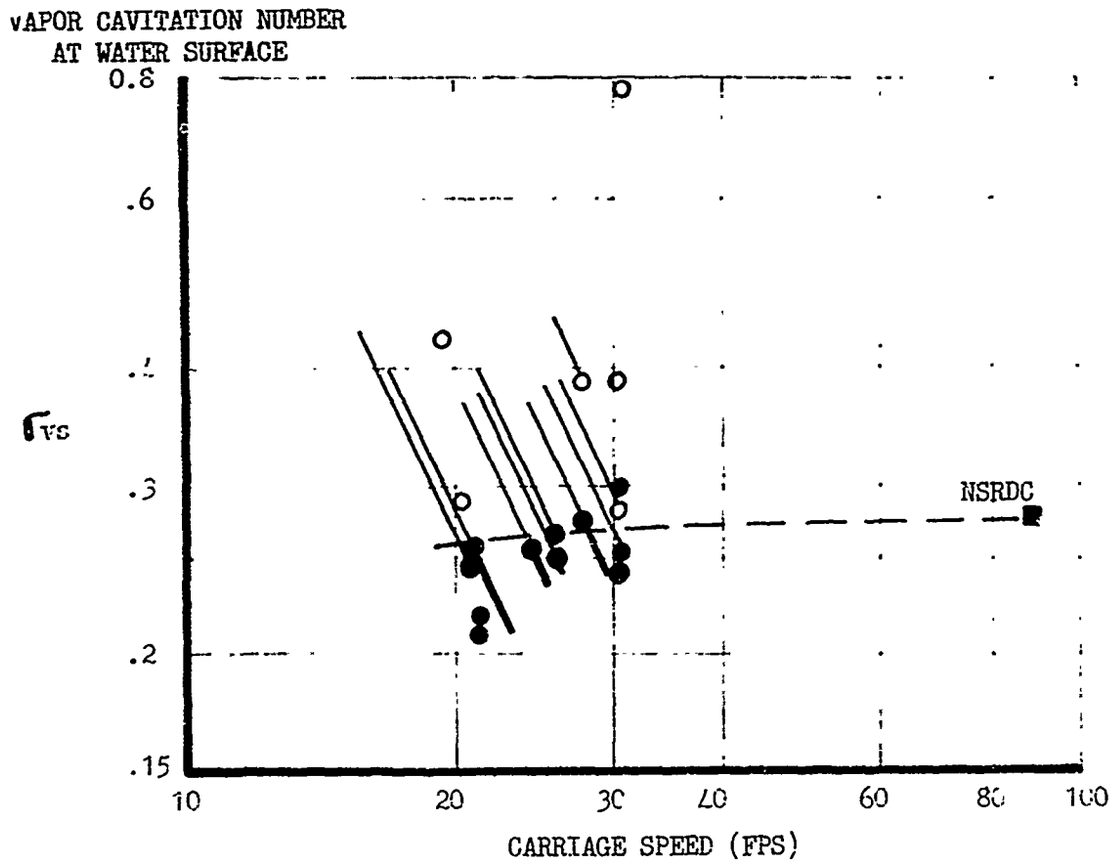

FIGURE 17. Conditions of flow for strut model 2 at a yaw angle of -8 degrees and a submergence of 1.0 chords. (Solid symbol indicates ventilation).

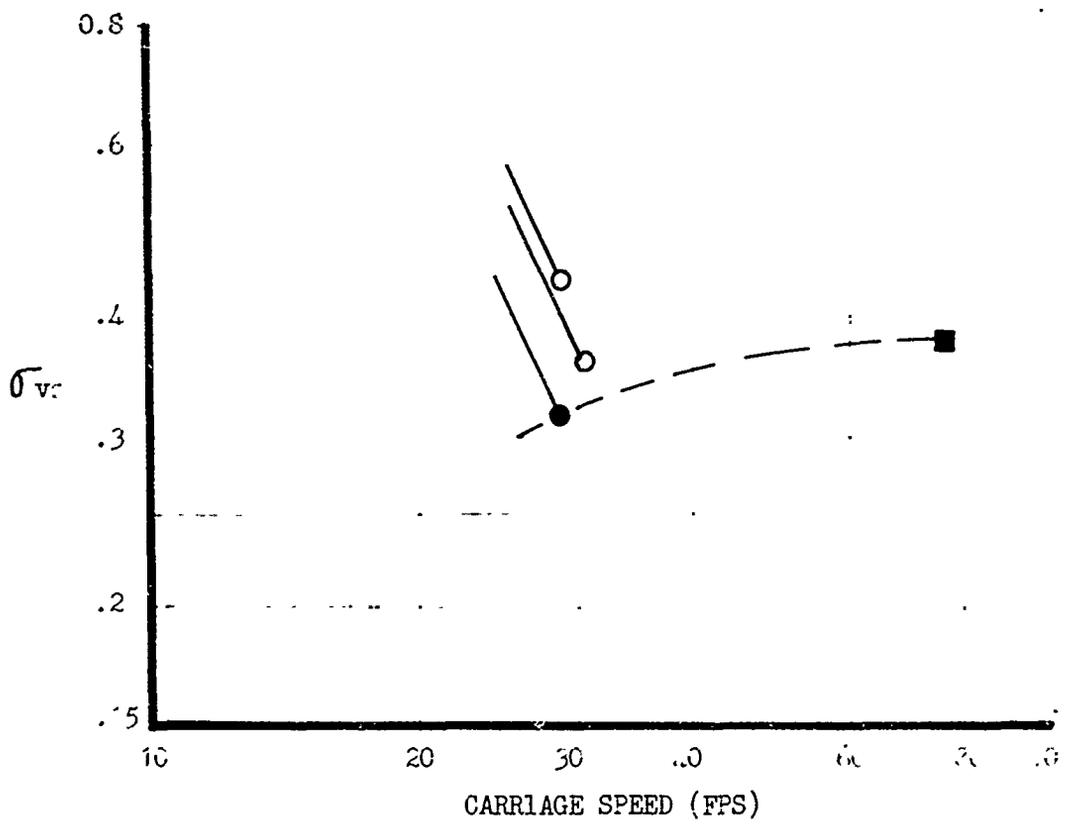

FIGURE 18. Conditions of flow for strut model 2 at a yaw angle of -10 degrees and a submergence of 1.0 chords. (Solid symbol indicates ventilation).

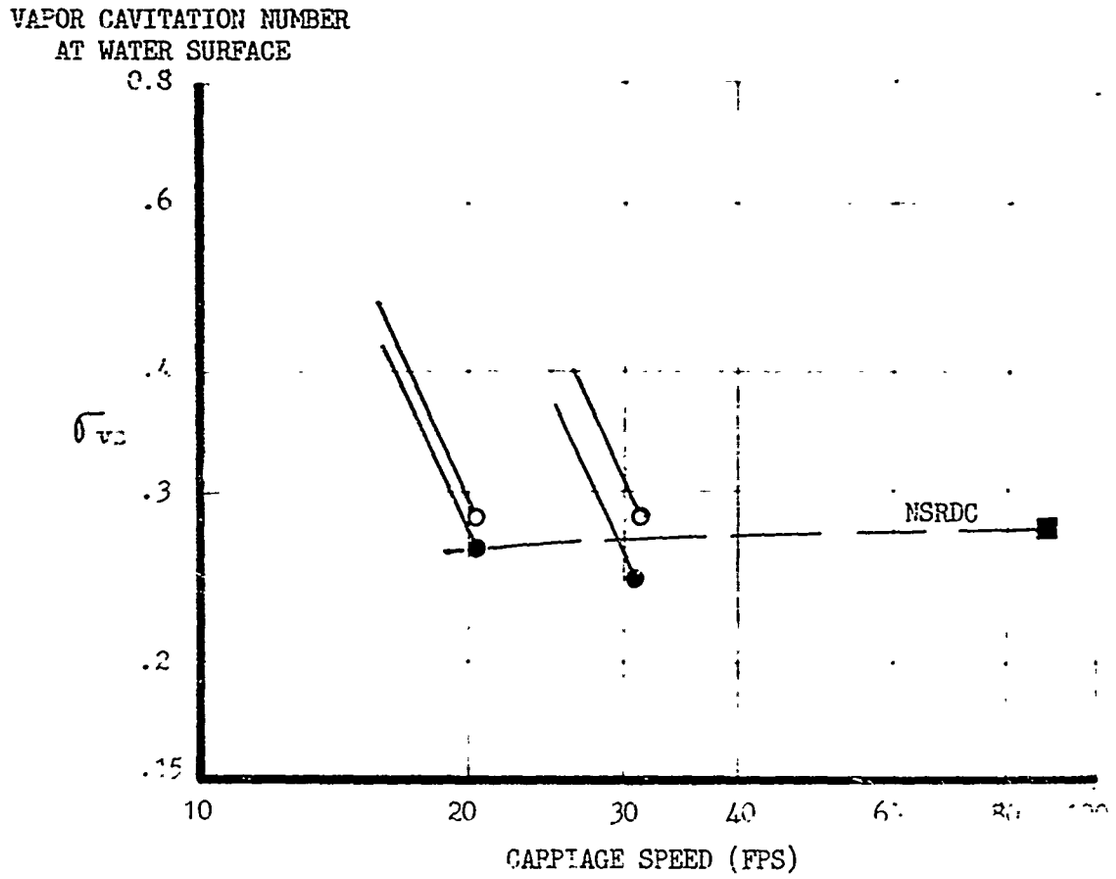

FIGURE 19. Conditions of flow for strut model 2 at a yaw angle of -8 degrees and a submergence of 1.5 chords. (Solid symbol indicates ventilation).

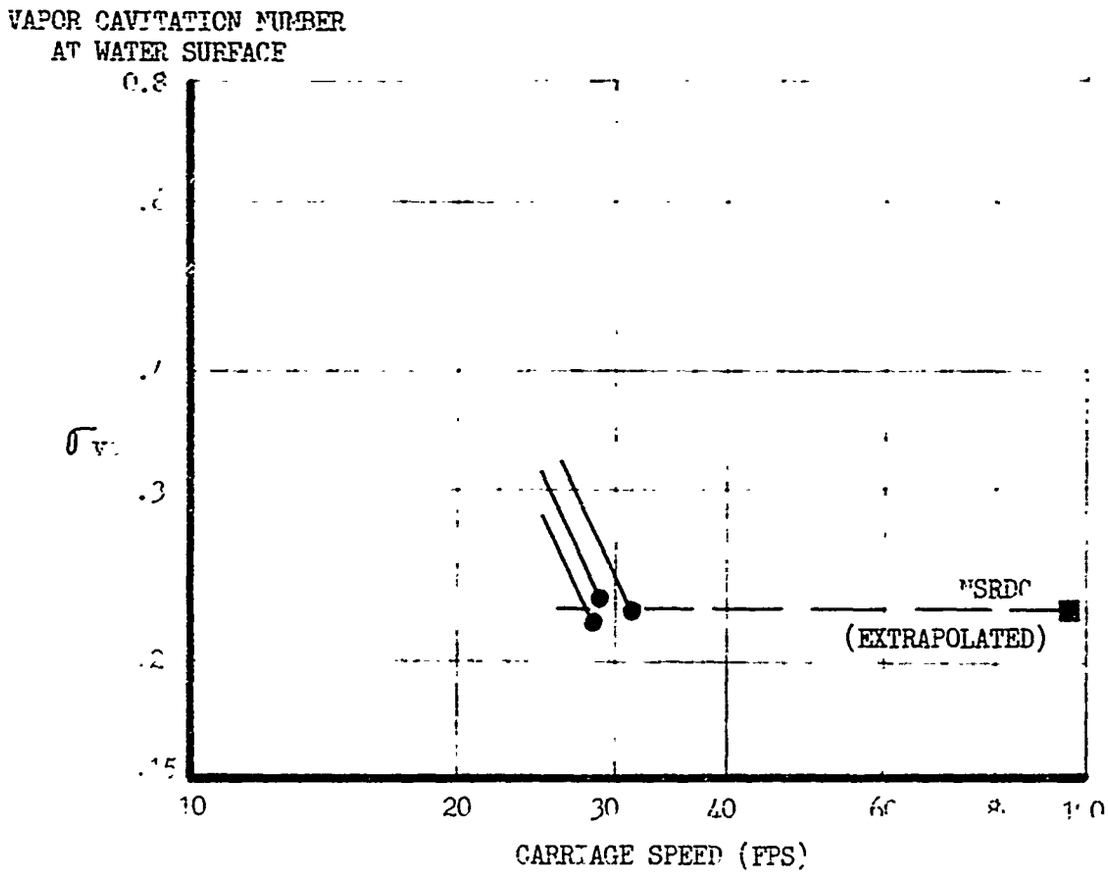

FIGURE 20 Conditions of flow for strut model 3 at a yaw angle of -6 degrees and a submergence of 1.0 chords. (Solid symbol indicates ventilation).

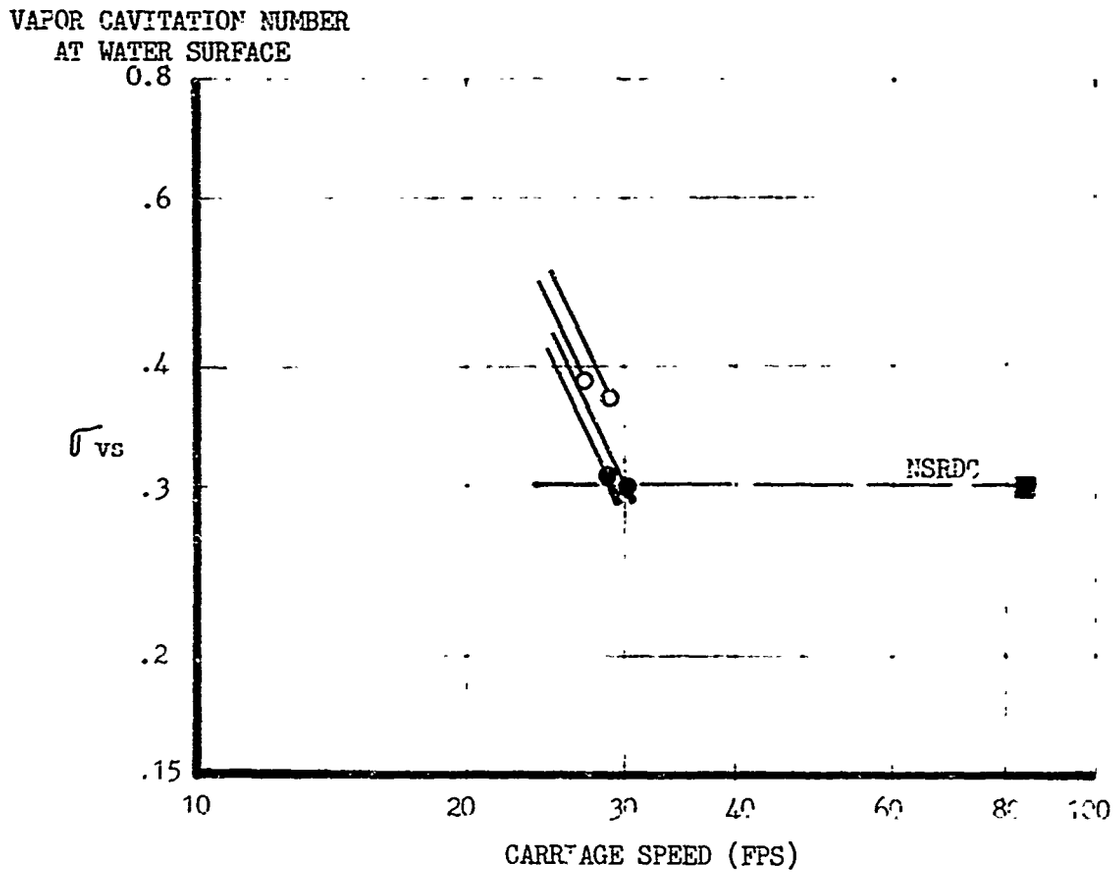

FIGURE 21 Conditions of flow for strut model 3 at a yaw angle of -8 degrees and a submergence of 1.0 chords. (Solid symbol indicates ventilation).

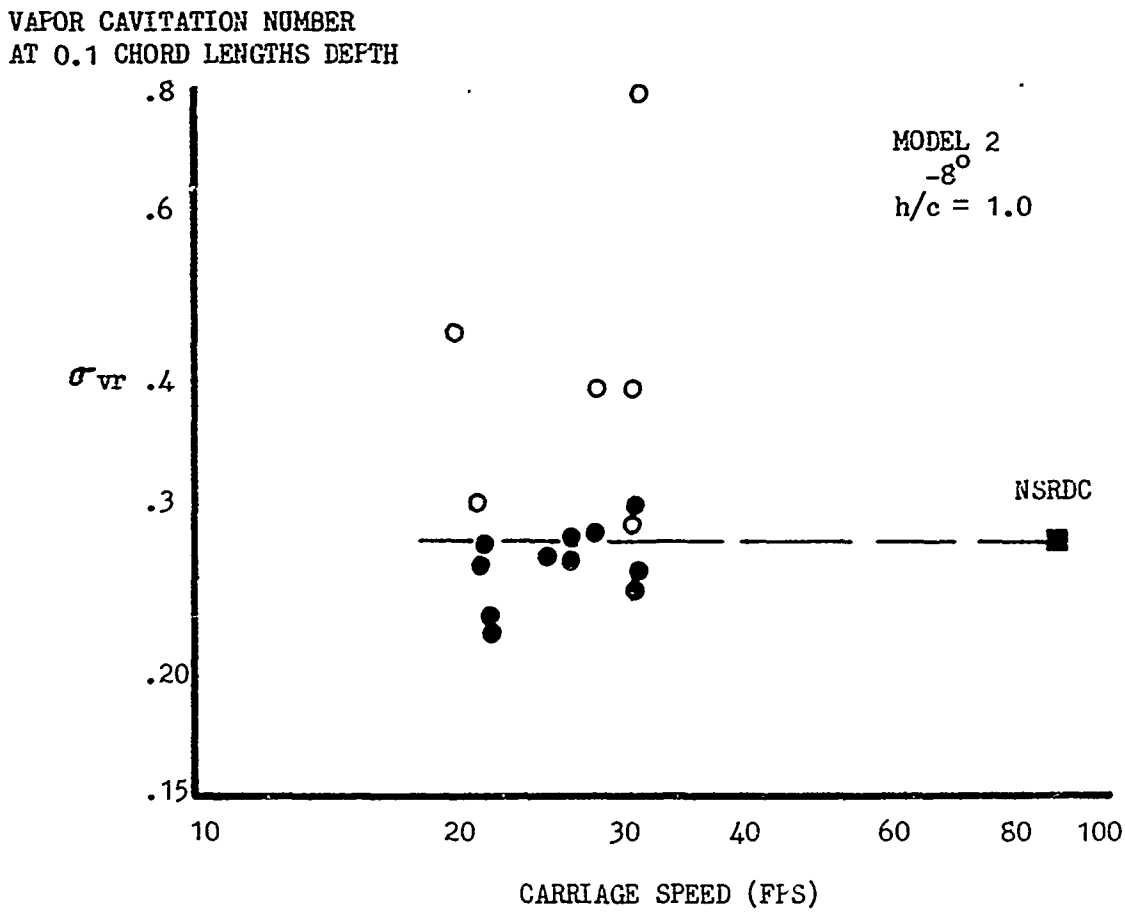

FIGURE 22. Conditions for ventilation inception of strut model 2 based on the vapor cavitation number at a representative depth (0.1 chord lengths). (Solid symbols indicate ventilation)

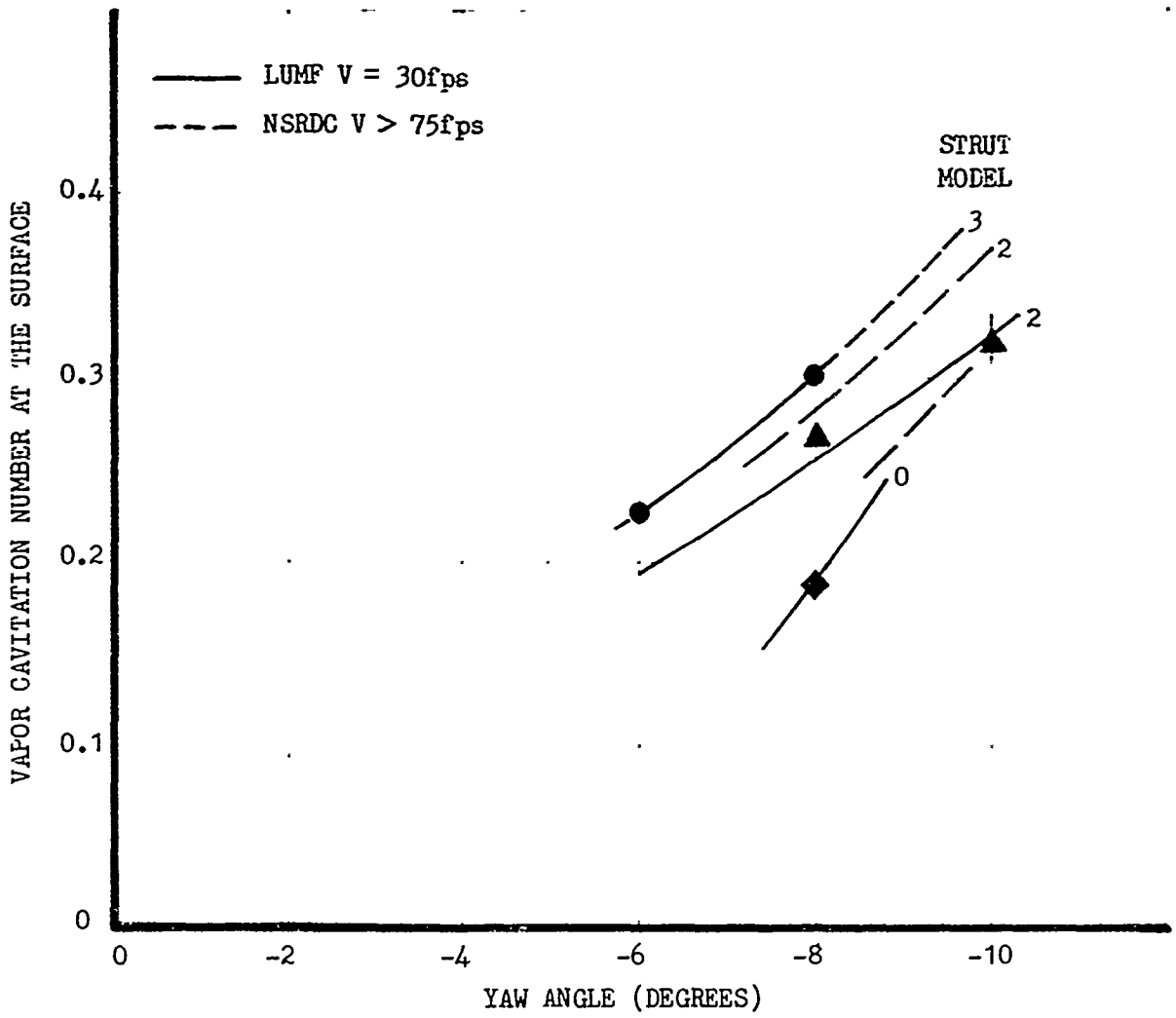

FIGURE 23. Vapor cavitation number for incipient ventilation at a submergence of 1.0 chord lengths.

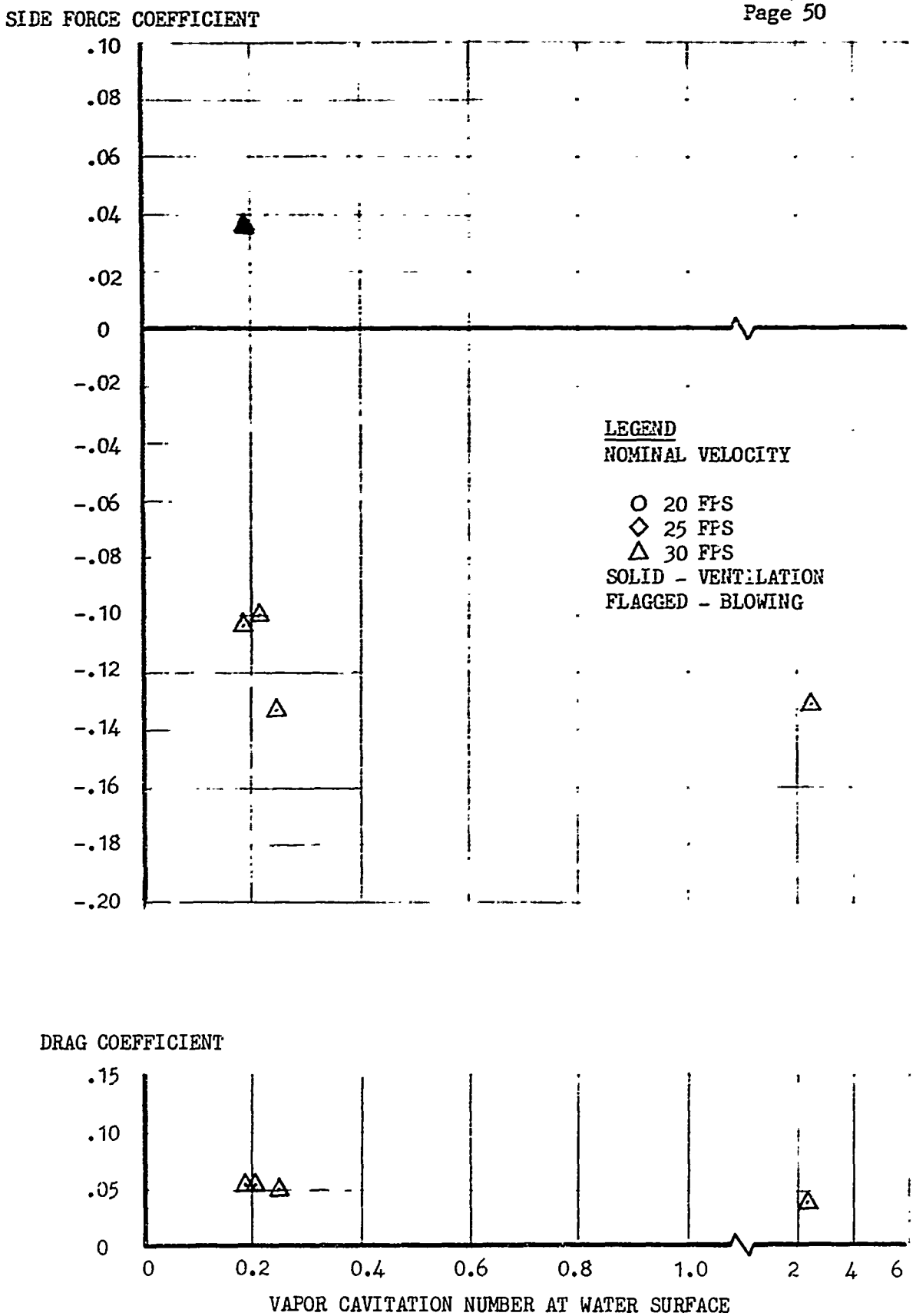

FIGURE 24: Side force and drag coefficient for strut model 0 at a yaw angle of -8 degrees and a submergence of 1.0 chord lengths.

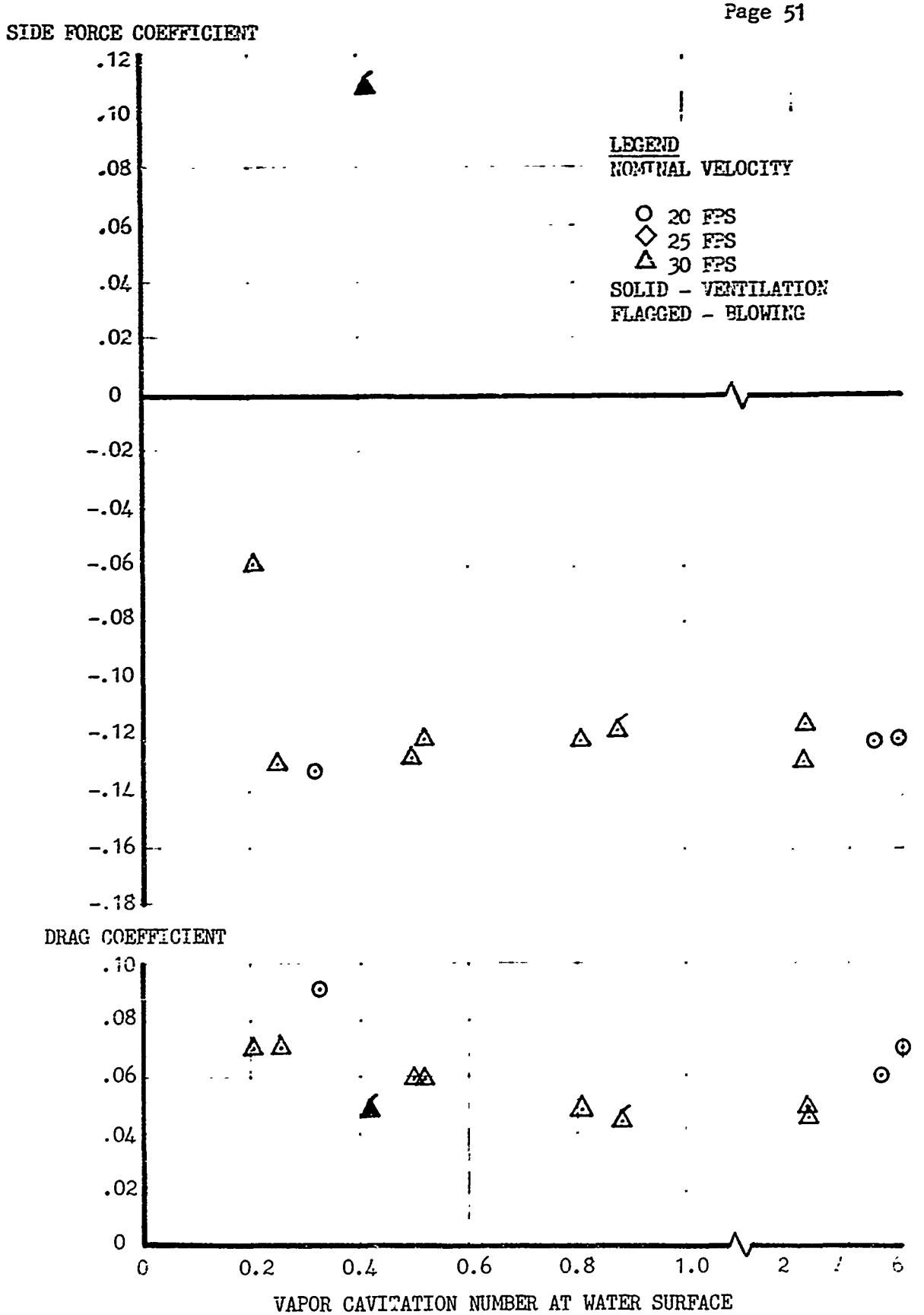

FIGURE 25: Side force and drag coefficient for strut model 2 at a yaw angle of -6 degrees and a submergence of 1.0 chord lengths.

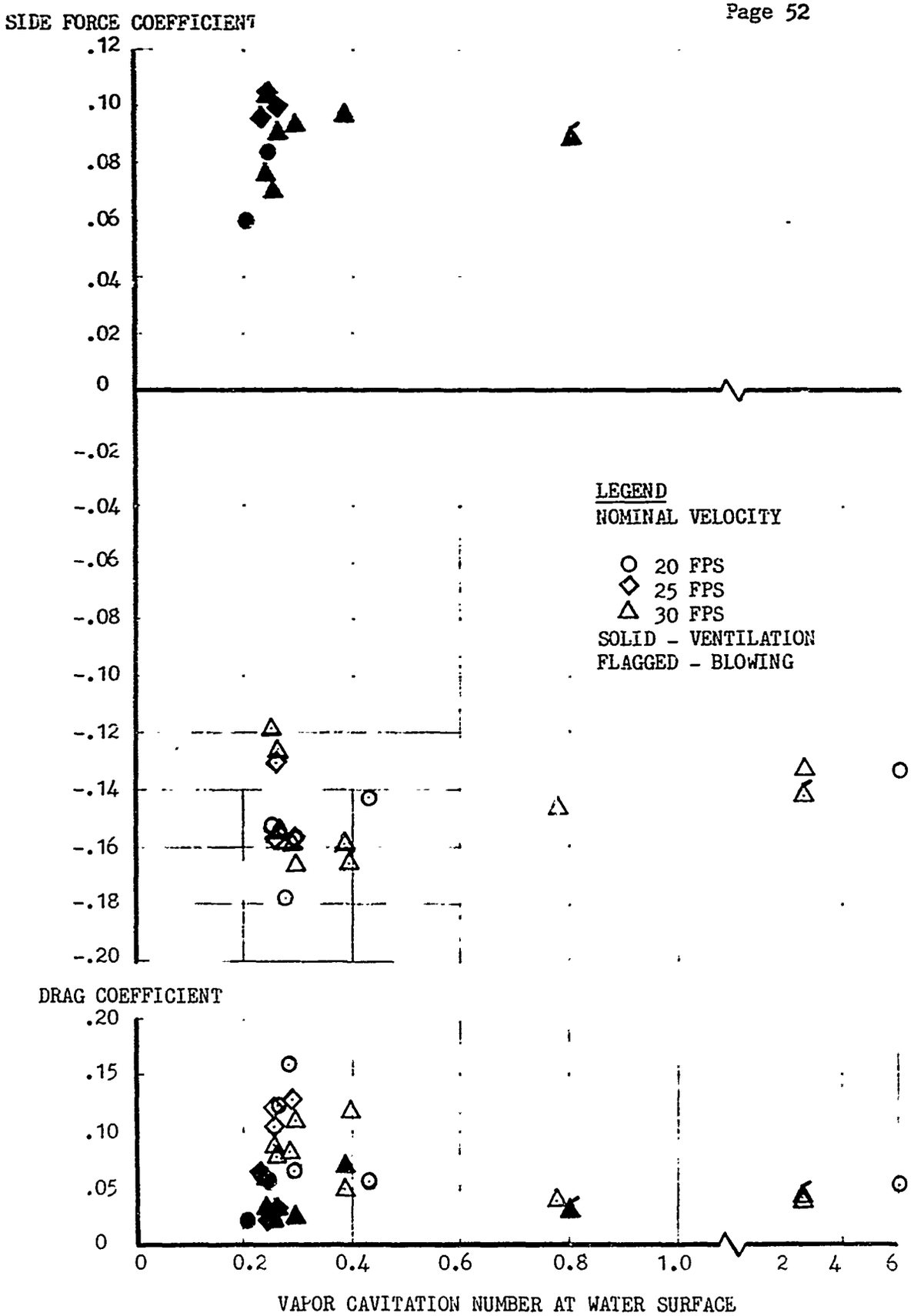

Figure 26 : Side force and drag coefficient for strut model 2 at a yaw angle of -8 degrees and a submergence of 1.0 chord lengths.

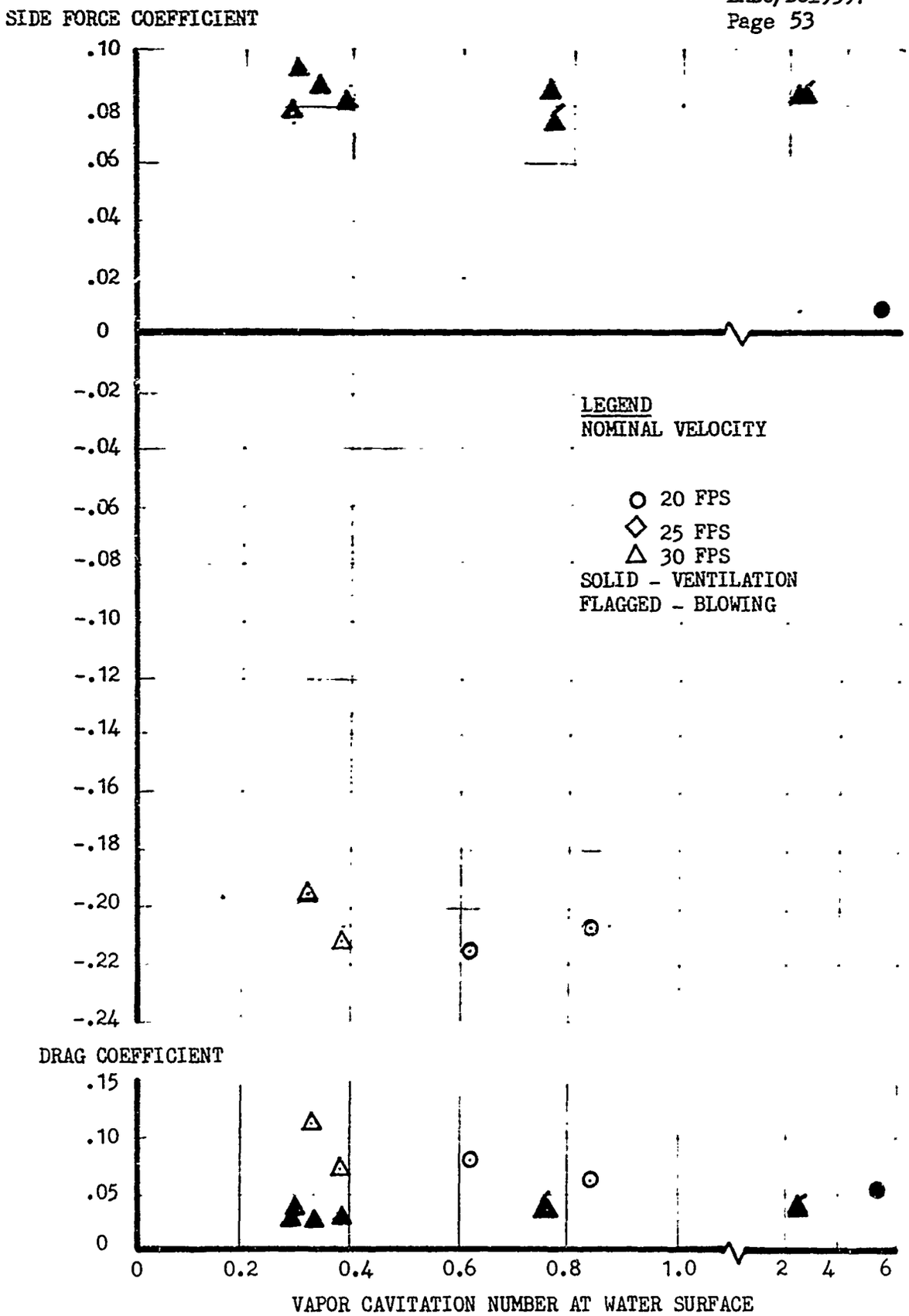

FIGURE 27. Side force and drag coefficient for strut model 2 at a yaw angle of -10 degrees and a submergence of 1.0 chord lengths.

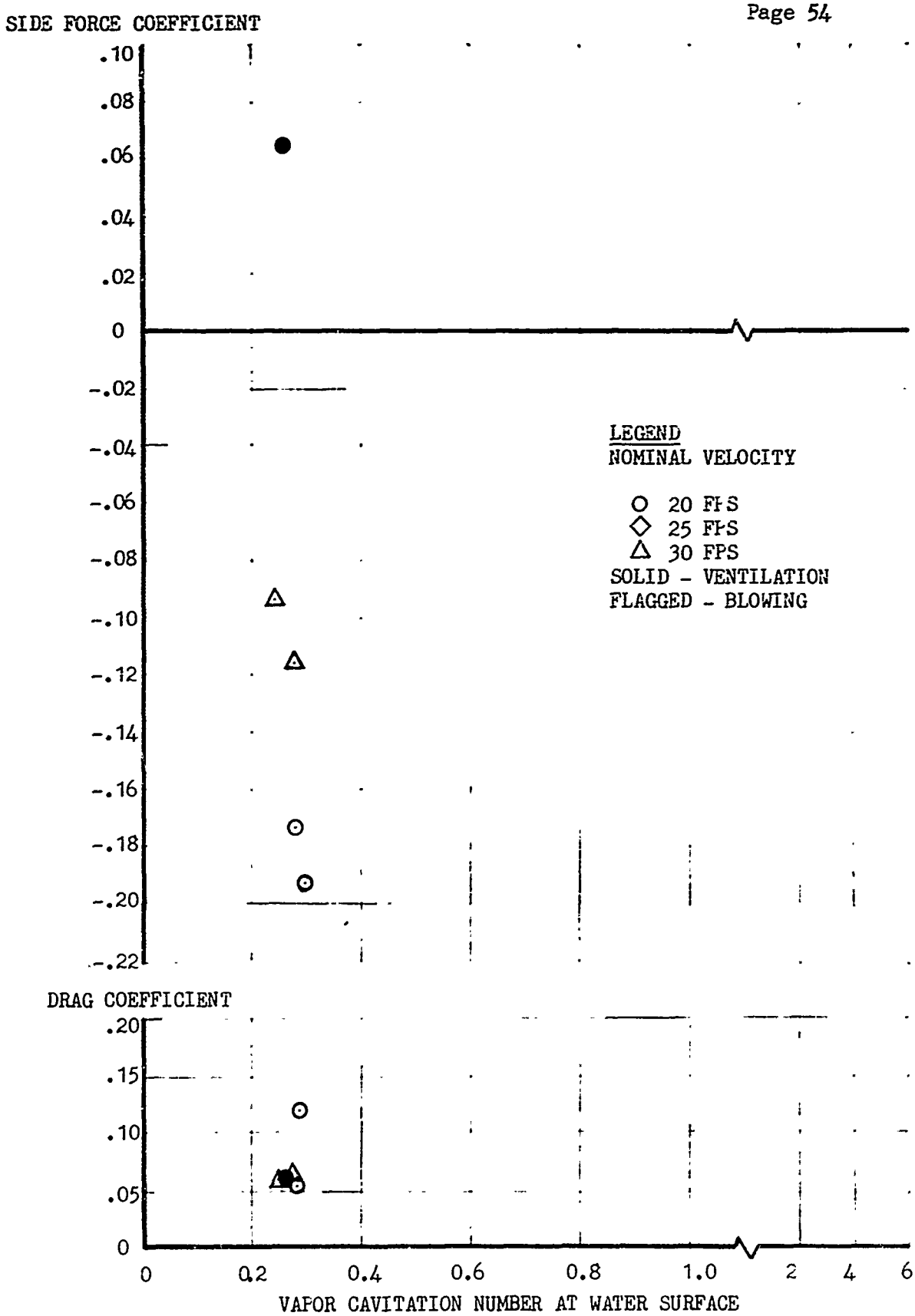

FIGURE 28: Side force and drag coefficient for strut model 2 at a yaw angle of -8 degrees and a submergence of 1.5 chord lengths.

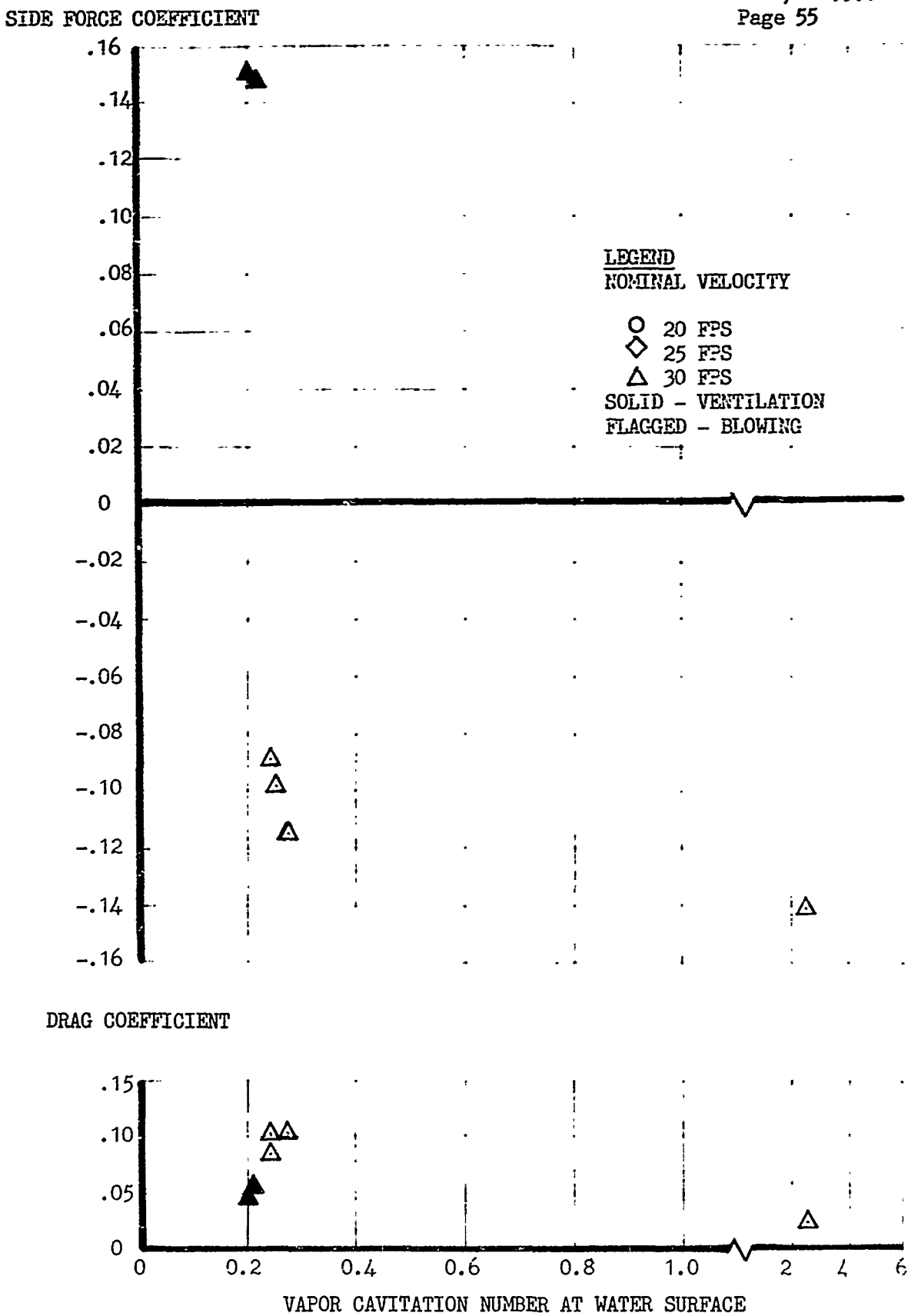

FIGURE 29: Side force and drag coefficient for strut model 3 at a yaw angle of -6 degrees and a submergence of 1.0 chord lengths

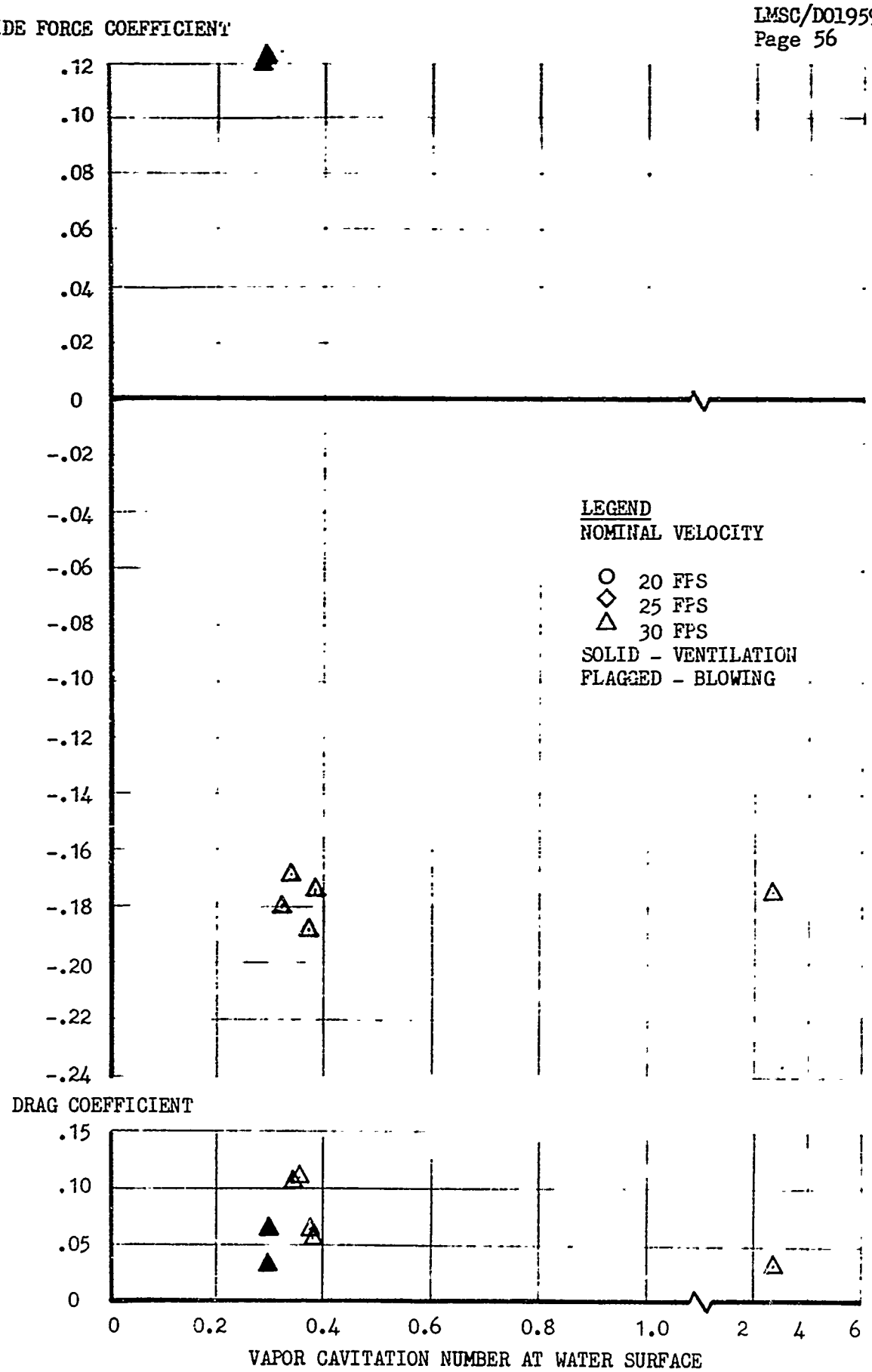

FIGURE 30: Side force and drag coefficient for strut model 3 at a yaw angle of -8 degrees and a submergence of 1.0 chord lengths.

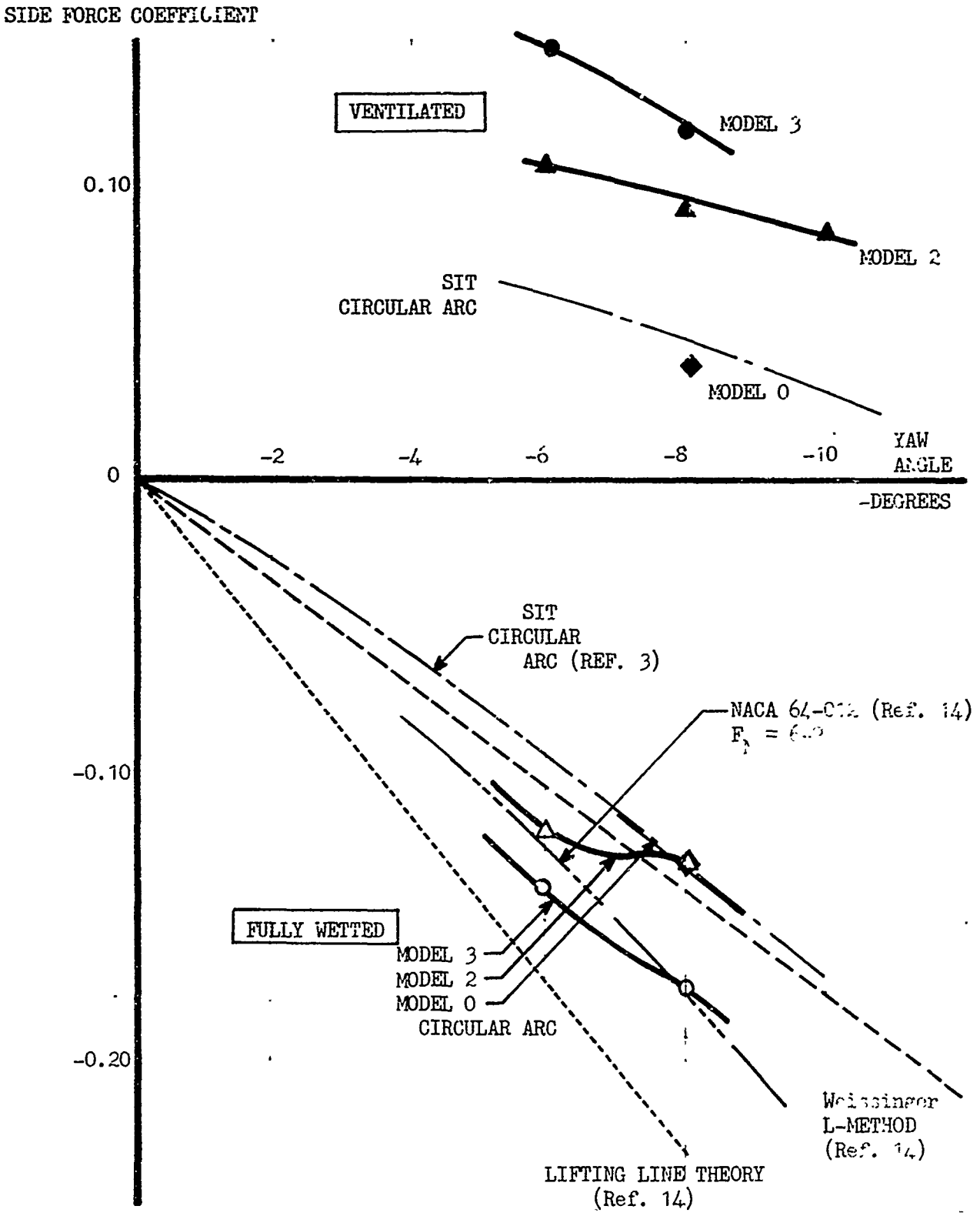

FIGURE 31. Average side force coefficients as a function of yaw angle for strut models 0, 2, and 3 at a submergence of 1.0 chord lengths for a velocity of 30 feet per second. (F_N = 5.3)